Refined Bounds on MeV-scale Thermal Dark Sectors from BBN and the CMB

Nashwan Sabti[$], James Alvey[A], Miguel Escudero[E], Malcolm Fairbairn[F], and Diego Blas[B]

Theoretical Particle Physics and Cosmology Group
King's College London, Department of Physics, Strand, London WC2R 2LS, UK

New light states thermally coupled to the Standard Model plasma alter the expansion history of the Universe and impact the synthesis of the primordial light elements. In this work, we carry out an exhaustive and precise analysis of the implications of MeV-scale BSM particles in Big Bang Nucleosynthesis (BBN) and for Cosmic Microwave Background (CMB) observations. We find that BBN observations set a lower bound on the thermal dark matter mass of $m_\chi > 0.4 \, \text{MeV}$ at 2σ. This bound is independent of the spin and number of internal degrees of freedom of the particle, of the annihilation being s-wave or p-wave, and of the annihilation final state. Furthermore, we show that current BBN plus CMB observations constrain purely electrophilic and neutrinophilic BSM species to have a mass, $m_\chi > 3.7 \, \text{MeV}$ at 2σ. We explore the reach of future BBN measurements and show that upcoming CMB missions should improve the bounds on light BSM thermal states to $m_\chi > (10 - 15) \, \text{MeV}$. Finally, we demonstrate that very light BSM species thermally coupled to the SM plasma are highly disfavoured by current cosmological observations.

[$] nashwan.sabti@kcl.ac.uk
[A] james.alvey@kcl.ac.uk
[E] miguel.escudero@kcl.ac.uk
[F] malcolm.fairbairn@kcl.ac.uk
[B] diego.blas@kcl.ac.uk

I   Introduction

The nature of dark matter is still unknown and thermal relics associated with the electroweak scale are under increasing pressure from the LHC as well as from direct and indirect detection experiments [1–13]. Motivated by the fact that direct detection experiments are considerably less sensitive to sub-GeV dark matter particles, attention has naturally turned to lower mass alternatives [14–17].

From a theoretical perspective, MeV-scale thermal dark matter candidates were shown to be viable some years ago [18–20] and, since then, a large number of MeV-scale dark matter models have appeared in the literature, see e.g. [21–38]. Experimentally, with the aim of testing as many scenarios as possible [39], a complementary program has been developed to test the possible existence of MeV-scale dark matter particles and potential companions Beyond the Standard Model (BSM) [14–17]. Light dark matter particles and their potential mediators with the dark sector have been searched for at particle colliders [40–47], beam dump experiments [48–50], neutrino experiments [51–56], neutrino telescopes [57–59], as well as in direct [60–67] and indirect [68–70] dark matter detection experiments. Searches for light BSM species are not only carried out in terrestrial experiments, but a variety of astrophysical [71–76] and cosmological [77–84] constraints have been also derived on states with masses at the MeV scale. Up to now, however, all these searches have been unsuccessful. Future, ongoing and planned experiments are expected to cut into relevant regions of parameter space and perhaps yield a signal [14–17, 85–89].

Big Bang Nucleosynthesis (BBN) has been widely used as a probe of new physics [90–92]. BBN occurred when the Universe was about three minutes old, in the temperature range $10\,\mathrm{keV} \lesssim T \lesssim 1\,\mathrm{MeV}$, and therefore represents a key stage of the Universe that new states at the MeV scale can affect. Given the excellent agreement between observations and the Standard Model (SM) prediction of the primordial light nuclei abundances [93], strong constraints can be set on the masses and properties of new light particles. Similarly, the agreement of Cosmic Microwave Background (CMB) observations with a vanilla ΛCDM Universe [7] can be used to set strong constraints on light new physics.

In this work, we perform an exhaustive and robust analysis of the cosmological implications of MeV-scale particles that are thermally coupled to electrons, neutrinos or both in the early Universe. This has been studied in the past by a number of groups [94–103], but here we update and upgrade the constraints by:

- Using up-to-date measurements of the primordial element abundances [93] and Planck 2018 CMB observations [7].

- Accurately accounting for the early Universe evolution in the presence of MeV-scale states following [103, 104].

- Using the state-of-the-art Big Bang Nucleosynthesis code `PRIMAT` [105], which outputs the most accurate theoretical predictions for the helium and deuterium abundances to date. `PRIMAT` accounts for a variety of effects, such as up-to-date nuclear reaction rates, finite temperature corrections, incomplete neutrino decoupling and several other effects relevant to the proton-to-neutron conversion rates.

- Performing a pure BBN analysis on light MeV-scale states. Namely, we set a bound on the masses of different species by using only the primordial helium and deuterium abundances and by marginalizing over any possible value of the baryon energy density.

While we are mostly interested in constraining MeV-scale dark matter particles, our analysis applies more generally to any additional BSM particles that are in thermal equilibrium with the SM during BBN and with a mass in the MeV range. This includes dark matter particles and mediators with the dark sector. In practice, this equilibrium should be maintained at temperatures below that of neutrino decoupling $T_\nu^{\mathrm{dec}} \sim 2\,\mathrm{MeV}$ [106]. The requirement of being in thermal contact at least prior to neutrino decoupling restricts the couplings and masses of the particles we are able to constrain. For the case of weakly-interacting, stable, thermal BSM particles (WIMPs), it is well known that annihilation interactions with the SM plasma will decouple from chemical equilibrium at $T \sim m/20$ [107]. Hence, our analysis will apply to thermal WIMPs with $m \lesssim 20\,T_\nu^{\mathrm{dec}} \sim 40\,\mathrm{MeV}$. In the case of unstable particles that decay

into SM species, they will be in thermal equilibrium with the SM plasma during BBN, provided that their lifetime is $\tau \lesssim 0.1\,\mathrm{s}$. In other words, the lifetime should be shorter than the age of the Universe at the time of neutrino decoupling.

Our analysis will constrain particles that efficiently annihilate or decay into neutrinos or electrons/photons prior and during neutrino decoupling. This is the case if the interaction rate is larger than the expansion rate H at neutrino decoupling:

$$\Gamma \gtrsim H|_{T=T_\nu^{\mathrm{dec}}} \simeq 10\,\mathrm{s}^{-1}. \tag{1}$$

Throughout the text we will denote a generic BSM particle as χ. For a particle that annihilates into SM species, the rate is $\Gamma \sim n\langle \sigma v\rangle \sim g_\chi^2 g_{\mathrm{SM}}^2 T^3/(16\pi m_\chi^2)$ and our analysis will generally be sensitive to

$$\text{Stable Particles with} \qquad \sqrt{g_\chi g_{\mathrm{SM}}} \gtrsim 2\times 10^{-5}\sqrt{\frac{m_\chi}{\mathrm{MeV}}} \qquad\qquad \text{and} \qquad m_\chi \lesssim 20\,\mathrm{MeV}, \tag{2}$$

where g_χ and g_{SM} are coupling constants. If the χ particle is unstable, then $\Gamma \sim g_{\mathrm{SM}}^2 m_\chi/(4\pi)\,K_1(m_\chi/T_\nu^{\mathrm{dec}})$ – K_1 being a modified Bessel function of the first kind – and our analysis will constrain

$$\text{Unstable Particles with} \qquad g_{\mathrm{SM}} \gtrsim 5\times 10^{-10}\sqrt{\frac{m_\chi}{\mathrm{MeV}}}\left(1+\sqrt{\frac{\mathrm{MeV}}{m_\chi}}\right) \qquad \text{and} \qquad m_\chi \lesssim 20\,\mathrm{MeV}. \tag{3}$$

In summary, the bounds we derive in this paper will generically constrain MeV-scale particles coupled to the SM bath with couplings $\gtrsim 10^{-5}$ if they are stable[1] and with couplings as small as 10^{-9} if they are unstable. Note that our bounds will apply even if these unstable BSM particles decay into other BSM states, under the condition that they possess couplings $\gtrsim 10^{-9}$ to SM particles.

This paper is organized as follows: In Section II, we describe our modelling of the early Universe evolution with light BSM species coupled to the SM plasma at temperatures $1\,\mathrm{keV} < T < 30\,\mathrm{MeV}$. In Section III, we outline the cosmological data and statistical procedure used to set constraints on the masses and properties of particles in thermal equilibrium with neutrinos and/or electrons in the early Universe. In Section IV, we set a lower bound on the mass of purely electrophilic and neutrinophilic BSM species in thermal equilibrium with the SM plasma from a combination of BBN and CMB data. In Section V, we set constraints on BSM species that efficiently interact with both neutrinos and electrons/photons. In Section VI, we forecast future BBN and CMB constraints. In Section VII, we discuss the robustness of our bounds, how they are modified in the presence of additional species, mention certain particle physics scenarios for which they represent the most stringent constraints, and compare with previous literature. Finally, in Section VIII, we present our conclusions. Details regarding the modification to the BBN code, comparison to previous literature, complete sets of results, and our CMB forecasting methodology can be found in the Appendices IX.

II Cosmology with Light WIMPS

The implications of light, thermally coupled BSM particles with the SM plasma at temperatures $T \sim 1\,\mathrm{MeV}$ are twofold [94]: *i)* they contribute to the expansion rate of the early Universe and *ii)* they release entropy into the plasma. In addition, if the new particles interact with both neutrinos and electrons/photons, they would efficiently delay the process of neutrino decoupling [95, 103].

II.1 Temperature Evolution and Universe's Expansion

In order to accurately account for such effects we follow [103] and assume that all relevant species can be described by thermal distributions and characterized by a temperature T_i. We then calculate the evolution of neutrino decoupling in terms of the temperature of the neutrinos and electromagnetic components of the plasma. When a neutrinophilic

---

[1] This would cover well the case of thermal dark matter, for which $\sqrt{g_\chi g_{\mathrm{SM}}} \sim 10^{-3}\sqrt{\frac{m_\chi}{10\,\mathrm{MeV}}}\sqrt[4]{\frac{\langle \sigma v\rangle}{3\times 10^{-26}\,\mathrm{cm}^3/s}}$.

or electrophilic BSM particle is present, the differential equations governing the evolution of T_ν and T_γ read:

$$\text{Neutrinophilic} \begin{cases} \dfrac{dT_\nu}{dt} = -\dfrac{12H\rho_\nu + 3H(\rho_\chi + p_\chi) - 3\frac{\delta\rho_\nu}{\delta t}}{3\frac{\partial\rho_\nu}{\partial T_\nu} + \frac{\partial\rho_\chi}{\partial T_\nu}} , & \text{(4a)} \\[4mm] \dfrac{dT_\gamma}{dt} = -\dfrac{4H\rho_\gamma + 3H(\rho_e + p_e) + 3H\,T_\gamma\frac{dP_{\text{int}}}{dT_\gamma} + 3\frac{\delta\rho_\nu}{\delta t}}{\frac{\partial\rho_\gamma}{\partial T_\gamma} + \frac{\partial\rho_e}{\partial T_\gamma} + T_\gamma\frac{d^2 P_{\text{int}}}{dT_\gamma^2}} , & \text{(4b)} \end{cases}$$

$$\text{Electrophilic} \begin{cases} \dfrac{dT_\nu}{dt} = -\dfrac{12H\rho_\nu - 3\frac{\delta\rho_\nu}{\delta t}}{3\frac{\partial\rho_\nu}{\partial T_\nu}} , & \text{(5a)} \\[4mm] \dfrac{dT_\gamma}{dt} = -\dfrac{4H\rho_\gamma + 3H(\rho_e + p_e) + 3H(\rho_\chi + p_\chi) + 3H\,T_\gamma\frac{dP_{\text{int}}}{dT_\gamma} + 3\frac{\delta\rho_\nu}{\delta t}}{\frac{\partial\rho_\gamma}{\partial T_\gamma} + \frac{\partial\rho_e}{\partial T_\gamma} + \frac{\partial\rho_\chi}{\partial T_\gamma} + T_\gamma\frac{d^2 P_{\text{int}}}{dT_\gamma^2}} , & \text{(5b)} \end{cases}$$

where ρ_i and p_i correspond to the energy density and pressure of a given particle respectively, $H = \sqrt{(8\pi/3)\sum_i \rho_i/M_{\text{Pl}}^2}$ is the Hubble parameter, $M_{\text{Pl}} = 1.22 \times 10^{19}\,\text{GeV}$ the Planck mass, and P_{int} and its derivatives account for finite temperature corrections. The reader is referred to [103] for further details. Here, $\delta\rho_\nu/\delta t$ corresponds to the energy exchange rate between neutrinos and electrons. Accounting for Fermi-Dirac statistics in the rates and setting $m_e = 0$, it reads [104]:

$$\left.\frac{\delta\rho_\nu}{\delta t}\right|_{\text{SM}} = \frac{G_F^2}{\pi^5}\left(1 - \frac{4}{3}s_W^2 + 8s_W^4\right) \times \left[32\,f_a^{\text{FD}}\left(T_\gamma^9 - T_\nu^9\right) + 56\,f_s^{\text{FD}}\,T_\gamma^4\,T_\nu^4\,(T_\gamma - T_\nu)\right] , \tag{6}$$

where $s_W^2 = 0.223$ [93], G_F is Fermi's constant, $f_a^{\text{FD}} = 0.884$, $f_s^{\text{FD}} = 0.829$, and we account for the electron mass as in [104].

We solve Equations (4a) – (5b) for $1\,\text{keV} < T_\gamma < 30\,\text{MeV}$. We start the integration at $t_0 = 1/(2H)|_{T=30\,\text{MeV}}$ for which we use as an initial condition $T_\gamma = T_\nu = 30\,\text{MeV}$, since for such high temperatures SM neutrino-electron interactions are highly efficient. By solving this set of differential equations, we find all the key background evolution quantities as a function of time, scale factor and temperature. In addition, we evaluate the number of effective relativistic degrees of freedom N_{eff} as relevant for CMB observations,

$$N_{\text{eff}} \equiv \frac{8}{7}\left(\frac{11}{4}\right)^{4/3}\left(\frac{\rho_{\text{rad}} - \rho_\gamma}{\rho_\gamma}\right) = 3\left(\frac{11}{4}\right)^{4/3}\left(\frac{T_\nu}{T_\gamma}\right)^4 , \tag{7}$$

where in the last step we have assumed that $\rho_{\text{rad}} = \rho_\nu + \rho_\gamma$. By solving this system of equations in the SM we find $N_{\text{eff}}^{\text{SM}} = 3.046$ [104], a result that is in perfect agreement with state-of-the-art calculations [108, 109].

Finally, if the χ particle interacts with both electrons and neutrinos, an additional energy exchange between the latter two particles should be included. Considering a stable particle and neglecting scattering interactions, this reads [103]:

$$\left.\frac{\delta\rho_\nu}{\delta t}\right|_\chi = \frac{g_\chi^2 m_\chi^5}{4\pi^4}\left(\langle\sigma v\rangle_{\chi\chi\to\bar\nu\nu}\left[T_\nu^2\,K_2^2\left[\frac{m_\chi}{T_\nu}\right] - T_\chi^2\,K_2^2\left[\frac{m_\chi}{T_\chi}\right]\right] - \langle\sigma v\rangle_{\chi\chi\to e^+e^-}\left[T_\chi^2\,K_2^2\left[\frac{m_\chi}{T_\chi}\right] - T_\gamma^2\,K_2^2\left[\frac{m_\chi}{T_\gamma}\right]\right]\right) . \tag{8}$$

For a thermal WIMP $\langle\sigma v\rangle_{\chi\chi\to e^+e^-} + \langle\sigma v\rangle_{\chi\chi\to\bar\nu\nu} = \langle\sigma v\rangle_{\text{WIMP}} \simeq 3 \times 10^{-26}\,\text{cm}^3/\text{s}$ [110]. If the particle annihilates predominantly to electrons, i.e. $\langle\sigma v\rangle_{\chi\chi\to e^+e^-} > \langle\sigma v\rangle_{\chi\chi\to\bar\nu\nu}$, then $T_\chi = T_\gamma$ and vice versa for neutrinos. In scenarios where we consider stable particles interacting with both electrons and neutrinos we shall fix the total annihilation cross section to $\langle\sigma v\rangle_{\text{WIMP}}$.

II.2 Primordial Nucleosynthesis in the Presence of Thermal BSM Particles

MeV-scale thermal relics affect the synthesis of the light elements, see e.g. [94–98]. In this work, we have modified the publicly available state-of-the-art BBN code `PRIMAT` [105] to accommodate for the presence of light BSM particles in thermal equilibrium with the SM plasma. This is done by computing the background cosmology externally using `NUDEC_BSM` [103, 104] and then passing on the relevant parameters[2] to the section of `PRIMAT` that takes care of the

---

[2] This includes the evolution as a function of time and scale factor of T_γ, T_ν, H and the residual entropy transfer between neutrinos and electrons as parametrized by $\mathcal{N}$ in `PRIMAT` [105].
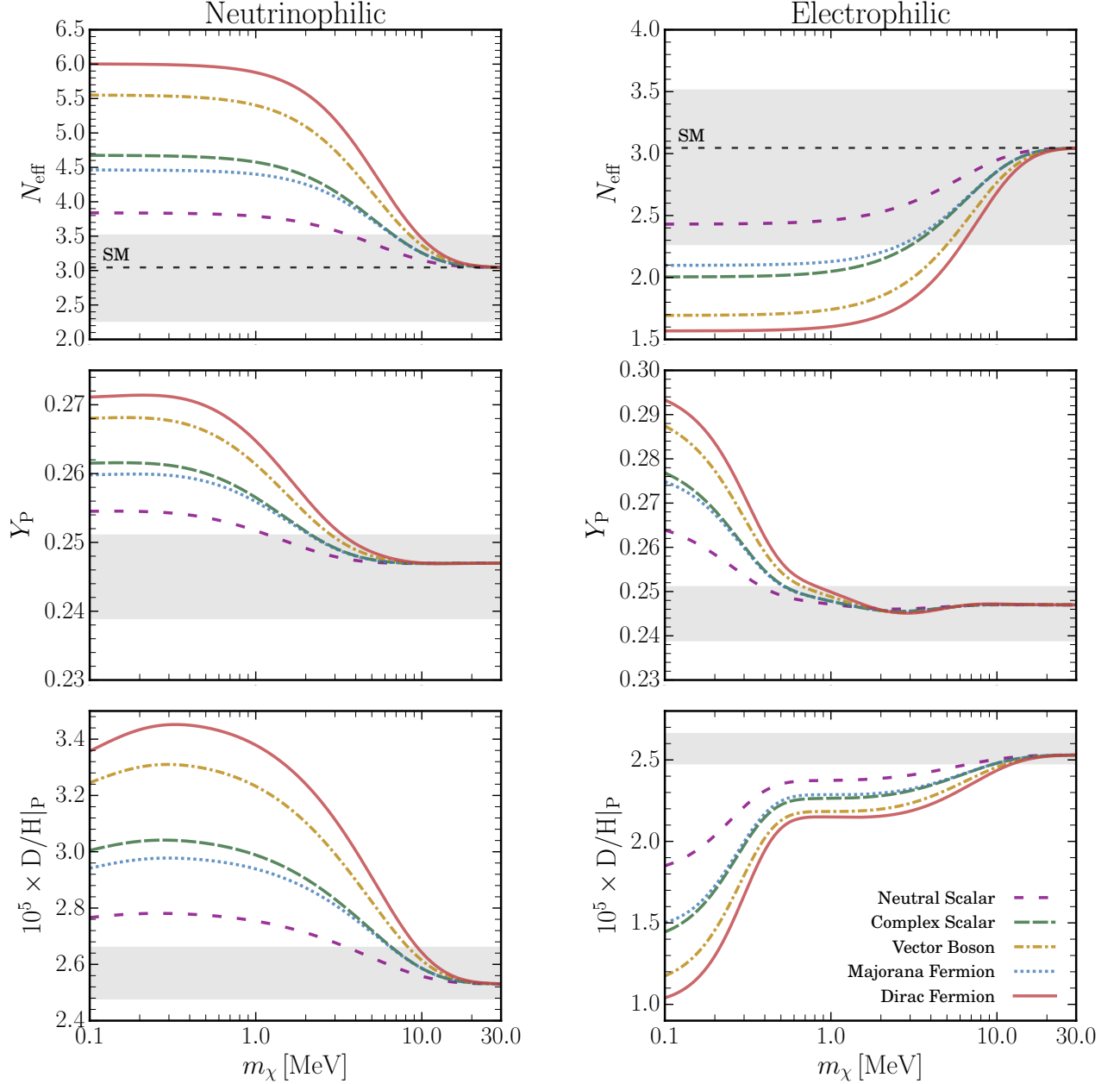
FIG. 1. Cosmological impact of light BSM particles in thermal equilibrium with the SM plasma as a function of their mass m_χ. The *left/right panel* corresponds to neutrinophilic/electrophilic particles. *Upper panels:* The number of effective relativistic neutrino species $N_{\rm eff}$ as relevant for CMB observations. *Middle panels:* Primordial helium abundance $Y_{\rm P}$. *Lower panels:* Primordial deuterium abundance D/H|$_{\rm P}$. The $Y_{\rm P}$ and D/H|$_{\rm P}$ predictions are computed with $\Omega_{\rm b}h^2 = 0.021875$ and $\tau_n = 879.5\,{\rm s}$. The grey contours correspond to the mean $\pm 2\sigma$ measurements that enter our BBN and Planck data analyses, see Eqs. (13), (14) and (15).

nuclear reaction rates and the time evolution of nuclei abundances. We have explicitly verified that the differences in the primordial element abundances between the default version of `PRIMAT` and with the SM evolution as calculated in [103, 104] are below 0.1 %, and hence one order of magnitude smaller than current observational errors. Our results agree quantitatively and qualitatively with previous studies [94–98][3] modulo differences we attribute to updated nuclear reaction rates and the fact that we account for non-instantaneous neutrino decoupling, see Appendix B for details.

---

[3] We agree particularly well with [97, 98], see Appendix B.

II.3 Cosmological Implications

In this section we review the main cosmological implications of light BSM particles in thermal equilibrium with the Standard Model plasma during neutrino decoupling and Big Bang Nucleosynthesis. The reader is referred to [94–98] for previous and complementary discussions of the impact of such particles on BBN and the CMB and to [90–92] for reviews on the role of BBN as a probe of physics beyond the Standard Model.

Cosmic Microwave Background – Modifications to $N_{\rm eff}$

Once neutrinos decouple from the SM plasma at $T_\nu^{\rm dec} \lesssim 2\,{\rm MeV}$, a light, neutrinophilic BSM particle of mass $m_\chi \lesssim 20\,{\rm MeV}$ will annihilate/decay into neutrinos, which results in $\rho_\nu > \rho_\nu^{\rm SM}$ or equivalently $N_{\rm eff} > N_{\rm eff}^{\rm SM}$. Analogously, an electrophilic particle will dump energy into the electromagnetic sector of the plasma at temperatures $T < T_\nu^{\rm dec}$ and yield $N_{\rm eff} < N_{\rm eff}^{\rm SM}$. In the upper panel of Figure 1, we display the corresponding value of $N_{\rm eff}$ for neutrinophilic and electrophilic BSM particles in thermal equilibrium with the SM plasma as a function of their mass. The grey contours correspond to the $\pm 2\sigma$ measurements by Planck (see below). With the sole exception of an electrophilic scalar particle, it is clear that regardless of what the spin and number of internal degrees of freedom of a given species are, Planck would set a lower bound on its mass.

Big Bang Nucleosynthesis

Light BSM particles in thermal equilibrium during BBN lead to three main effects on the cosmological evolution that impact the synthesis of the primordial elements. Firstly, additional species present in the early Universe will alter the expansion rate and therefore also the temperature-to-time relation. This is important because they will modify the time at which various weak and nuclear processes freeze-out, in particular the proton-to-neutron conversion and $p+n \leftrightarrow D+\gamma$. Secondly, the presence of these particles can change the evolution of the neutrino-to-photon temperature ratio. This has relevant implications because this ratio enters the proton-to-neutron conversion rates. Finally, light species thermally coupled to the electromagnetic sector of the plasma will release entropy after nucleosynthesis and therefore dilute the number density of all nuclei for a given primordial baryon-to-photon ratio. The impact of the particles considered in this work on the primordial abundances of helium and deuterium is depicted in the middle and lower panels of Figure 1 and can be suitably categorised into three mass regions:

A. $m_\chi \lesssim 0.05\,{\rm MeV}$
Very light neutrinophilic particles simply contribute to the expansion rate of the Universe during BBN, and do not alter the baryon-to-photon ratio. As such, they simply shorten the timescales on which the weak and nuclear processes freeze out, increasing both $Y_{\rm P}$ – which is approximately proportional to the neutron-to-proton ratio at $T \sim 0.07\,{\rm MeV}$ [90–92] – and D/H$|_{\rm P}$ relative to the SM. Whilst very light electrophilic particles contribute to the expansion rate, which increases the value of $Y_{\rm P}$, they also release substantial amounts of entropy into the electromagnetic plasma *after* nucleosynthesis. This acts to dilute number of baryons per photon and hence leads to a smaller value of D/H$|_{\rm P}$ than in the SM.

B. $0.5\,{\rm MeV} \lesssim m_\chi \lesssim 10\,{\rm MeV}$
Electrophilic particles in this region lead to a smaller energy density of the Universe during nucleosynthesis and again to entropy release. This leads to lower values for both $Y_{\rm P}$ and D/H$|_{\rm P}$ as is seen in the lower two panels of Figure 1. For neutrinophilic particles on the other hand, there is a larger energy density than in the SM, and hence a larger expansion rate. This leads to larger values for both $Y_{\rm P}$ and D/H$|_{\rm P}$ for a given $\Omega_{\rm b}h^2$.

C. $m_\chi \gtrsim 30\,{\rm MeV}$
In this region of masses the energy density of the particles at the time of nucleosynthesis is negligible since their number density is Boltzmann suppressed. As such, one recovers the SM predictions for the primordial element abundances.

Of course, the abundances of other light elements like ^{3}He or ^{7}Li are also affected by the presence of light thermal BSM particles. However, such abundances are not typically used as cosmological probes [93], and therefore we do not use them in this work. The interested reader is referred to Appendix E for the effect of different types of thermal BSM particles on these abundances.

Expectations

From Figure 1 we notice that thermal species of mass $m_\chi \lesssim 0.4-3\,{\rm MeV}$ will be ruled out by current $Y_{\rm P}$ measurements. Note that $Y_{\rm P}$ is only logarithmically dependent upon the baryon energy density $\Omega_{\rm b}h^2$. One might also expect current D/H$|_{\rm P}$ measurements to set stringent constraints on the mass of various BSM particles; about $m_\chi \lesssim 3-10\,{\rm MeV}$. However, note that the D/H$|_{\rm P}$ predictions are shown for a fixed value of $\Omega_{\rm b}h^2$ and D/H$|_{\rm P}$ is strongly sensitive to $\propto \Omega_{\rm b}h^2$, thus deuterium measurements will only yield constraints provided that $\Omega_{\rm b}h^2$ is inferred from CMB observations or in conjunction with $Y_{\rm P}$ measurements.

Analysis	Cosmological Data	Description
BBN	$(Y_{\mathrm{P}}, \mathrm{D/H}|_{\mathrm{P}})$	Mean values and error bars as recommended by the PDG. Theoretical uncertainties in the predictions are accounted for.
BBN+$\Omega_{\mathrm{b}}h^2$	$(Y_{\mathrm{P}}, \mathrm{D/H}|_{\mathrm{P}}, \Omega_{\mathrm{b}}h^2)$	Same as BBN but with $\Omega_{\mathrm{b}}h^2 = 0.02225 \pm 0.00066$ from CMB observations. This represents a conservative and model independent range for $\Omega_{\mathrm{b}}h^2$.
Planck	$(\Omega_{\mathrm{b}}h^2, N_{\mathrm{eff}}, Y_{\mathrm{P}})$	From the Planck2018-TTTEEE+lowE analysis. Assumes ΛCDM + varying N_{eff} and Y_{P}.
Planck+H_0	$(\Omega_{\mathrm{b}}h^2, N_{\mathrm{eff}}, Y_{\mathrm{P}})$	From the Planck2018-TTTEEE+lowE+lensing+BAO+H_0 analysis. Assumes ΛCDM + varying N_{eff} and Y_{P}.
Planck+BBN	$(\Omega_{\mathrm{b}}h^2, N_{\mathrm{eff}}, Y_{\mathrm{P}})+$ $(Y_{\mathrm{P}}, \mathrm{D/H}|_{\mathrm{P}})$	Joint constraint from Planck 2018 CMB observations and Y_{P} and $\mathrm{D/H}|_{\mathrm{P}}$ determinations as recommended by the PDG.

TABLE I. Summary of the different baseline analyses carried out in this work in order to constrain light BSM particles in thermal equilibrium with the SM plasma during BBN. For each analysis, a likelihood is computed on a grid of $(\Omega_{\mathrm{b}}h^2, m_\chi)$.

III   Cosmological Data and Analysis

In order to set constraints on the masses of various BSM particles, we perform very conservative analyses using the latest determinations of the primordial element abundances and CMB observations by the Planck satellite as described below. Table I provides a summary of the main data sets used in each analysis.

III.1 Big Bang Nucleosynthesis

We use the PDG recommended means and error bars for the observed primordial abundances of helium and deuterium, which at 1σ read [93]:

$$Y_{\mathrm{P}} = 0.245 \pm 0.003\,, \tag{9}$$

$$\mathrm{D/H}|_{\mathrm{P}} = (2.569 \pm 0.027) \times 10^{-5}\,. \tag{10}$$

These values are based on the analyses/measurements of [111–113] and [114–117] for helium and deuterium respectively. In addition to the observational uncertainties in Y_{P} and $\mathrm{D/H}|_{\mathrm{P}}$, we account for theoretical uncertainties in the predicted abundances arising from uncertainties in the neutron lifetime[4] and various nuclear reaction rates. These are given by [105]:

$$\sigma(Y_{\mathrm{P}})^{\mathrm{Theo}} = 0.00017\,, \tag{11}$$

$$\sigma(\mathrm{D/H}|_{\mathrm{P}})^{\mathrm{Theo}} = 0.036 \times 10^{-5}\,. \tag{12}$$

Assuming Gaussian statistics and combining in quadrature the observational and theoretical errors, we define the following effective BBN χ^2:

$$\chi^2_{\mathrm{BBN}} = \frac{\left[Y_{\mathrm{P}} - Y_{\mathrm{P}}^{\mathrm{Obs}}\right]^2}{\sigma^2_{Y_{\mathrm{P}}}|^{\mathrm{Theo}} + \sigma^2_{Y_{\mathrm{P}}}|^{\mathrm{Obs}}} + \frac{\left[\mathrm{D/H}|_{\mathrm{P}} - \mathrm{D/H}|_{\mathrm{P}}^{\mathrm{Obs}}\right]^2}{\sigma^2_{\mathrm{D/H}|_{\mathrm{P}}}|^{\mathrm{Theo}} + \sigma^2_{\mathrm{D/H}|_{\mathrm{P}}}|^{\mathrm{Obs}}}\,, \tag{13}$$

which we will use to quantify deviations from the observed primordial abundances due to the presence of the new particles in the thermal bath.

III.2 Cosmic Microwave Background: Planck 2018

CMB observations measure very precisely three parameters that are relevant for our analysis: $\Omega_{\mathrm{b}}h^2$, N_{eff}, Y_{P}. The baryon abundance $\Omega_{\mathrm{b}}h^2$ is one of the 6 parameters in ΛCDM and Planck reports measurements on $\Omega_{\mathrm{b}}h^2$ with greater than 1% accuracy. N_{eff} represents one of the most important cosmological parameters and the current accuracy by

---

[4] Since we account for the uncertainty in the neutron lifetime, in all analyses presented in this work, we shall fix the neutron lifetime to the default value in PRIMAT: $\tau_n = 879.5\,\mathrm{s}$. This value is compatible with the PDG within 1σ, $\tau_n = 880.2 \pm 1\,\mathrm{s}$ [93]. Choosing $\tau_n = 880.2\,\mathrm{s}$ will not alter any of the results presented in this study.

the Planck satellite on this parameter is $\mathcal{O}(10\,\%)$. Y_{P} is also constrained by CMB observations, albeit with error bars that are typically a factor of 6 - 7 larger than those inferred from blue compact galaxies [93], see Equation (9).

In this work, we use the latest CMB observations by the Planck satellite to set constraints on the masses and interactions of various BSM particles. Since the disagreement between local [118] and CMB determinations of the Hubble constant [7] could potentially be attributed to additional contributions to N_{eff} [119, 120], we consider two data sets: $i)$ in which we consider the 2018 Planck baseline TTTEEE+lowE analysis and $ii)$ where we combine Planck CMB data with Baryon Acoustic Oscillation (BAO) measurements [121–123] and the local measurement of H_0 as reported by the SH0ES collaboration [118]. We shall call the former data set Planck and the latter Planck+H_0.

We build a Gaussian likelihood for the relevant parameters:

$$\chi^2_{\mathrm{CMB}} = (\Theta - \Theta_{\mathrm{Obs}})^T\, \Sigma^{-1}_{\mathrm{CMB}}\, (\Theta - \Theta_{\mathrm{Obs}})\,, \qquad \text{with} \qquad \Sigma_{\mathrm{CMB}} = \begin{pmatrix} \sigma_1^2 & \sigma_1\sigma_2\rho_{12} & \sigma_1\sigma_3\rho_{13} \\ \sigma_1\sigma_2\rho_{12} & \sigma_2^2 & \sigma_2\sigma_3\rho_{23} \\ \sigma_1\sigma_3\rho_{13} & \sigma_2\sigma_3\rho_{23} & \sigma_3^2 \end{pmatrix}\,, \qquad (14)$$

where $\Theta = (\Omega_{\mathrm{b}}h^2,\, N_{\mathrm{eff}},\, Y_{\mathrm{P}})$ and

$$\text{\textit{Planck 2018}} \qquad\qquad\qquad\qquad \text{\textit{Planck 2018+BAO+}}H_0$$

$$\begin{aligned} (\Omega_{\mathrm{b}}h^2,\, N_{\mathrm{eff}},\, Y_{\mathrm{P}})|_{\mathrm{Obs}} &= (0.02225,\, 2.89,\, 0.246), & (\Omega_{\mathrm{b}}h^2,\, N_{\mathrm{eff}},\, Y_{\mathrm{P}})|_{\mathrm{Obs}} &= (0.02345,\, 3.36,\, 0.249), \\ (\sigma_1,\, \sigma_2,\, \sigma_3) &= (0.00022,\, 0.31,\, 0.018), \quad (15) & (\sigma_1,\, \sigma_2,\, \sigma_3) &= (0.00025,\, 0.25,\, 0.020), \quad (16) \\ (\rho_{12},\, \rho_{13},\, \rho_{23}) &= (0.40,\, 0.18,\, -0.69)\,, & (\rho_{12},\, \rho_{13},\, \rho_{23}) &= (0.011,\, 0.50,\, -0.64)\,, \end{aligned}$$

where the covariance matrix for the Planck 2018 analysis has been extracted from the Planck database [7, 124]. The covariance matrix for the Planck 2018+BAO+H_0 analysis was obtained by running a Markov-Chain-Monte-Carlo analysis using `CLASS` [125, 126] and `Monte Python` [127, 128] with Planck 2018 data [7, 124], various BAO measurements [121–123] and by including a Gaussian likelihood on H_0 from the results of [118]. Clearly, the main implication of including local measurements of H_0 in the fit is the upward shift on the reconstructed value of N_{eff} from 2.89 to 3.36.

III.3 BBN+CMB Data Combinations

Combining measurements of the primordial element abundances and CMB observations proves useful in constraining light thermal species coupled to the SM plasma.

In this work, we will combine BBN+CMB data in two ways: $i)$ by constructing a joint χ^2 that is obtained by summing the individual Planck and BBN χ^2's as defined in Eqs. (13) and (14) (labelled BBN+Planck across the paper) and $ii)$ by adding to χ^2_{BBN} a measurement of $\Omega_{\mathrm{b}}h^2 = 0.02225 \pm 0.00066$, which is to be regarded as a cosmological model-independent Planck determination of the baryon energy density[5] (we shall call this analysis BBN+$\Omega_{\mathrm{b}}h^2$). See Appendix C for details.

III.4 Statistical Assessment

For each of the scenarios considered, the quantities χ^2_{BBN} and χ^2_{CMB} are computed on a grid of $(\Omega_{\mathrm{b}}h^2,\, m_\chi)$ and subsequently marginalized over $\Omega_{\mathrm{b}}h^2$. Then, by comparing the marginalized 1-D $\chi^2(m_\chi)$ with the minimum χ^2_{min}, we consider a scenario to be ruled out at 2σ when $\Delta\chi^2 \equiv \chi^2 - \chi^2_{\mathrm{min}} = 4$. The statistical compatibility of each χ^2_{min} is estimated by computing its p-value, which is found to be acceptable in all cases presented in this work. This is as expected, given that BBN predictions and CMB observations are compatible with each other within the Standard Model.

IV Current Cosmological Constraints on Purely Electrophilic or Neutrinophilic Species

Using different sets of cosmological observations, we set stringent constraints on the mass of various BSM species that are thermally coupled to the SM plasma. In Table I we provide a summary of the data sets used in each analysis, and in Table II we report the 95.4% CL lower bounds on the mass of such BSM species.

---

[5] The value $\Omega_{\mathrm{b}}h^2 = 0.02225 \pm 0.00066$ has an error 4.4 times larger than the one associated with ΛCDM using Planck 2018 observations [7], and furthermore it covers well the inferred value of $\Omega_{\mathrm{b}}h^2$ in a well-motivated 12-parameter extension of ΛCDM using different data sets [129, 130].
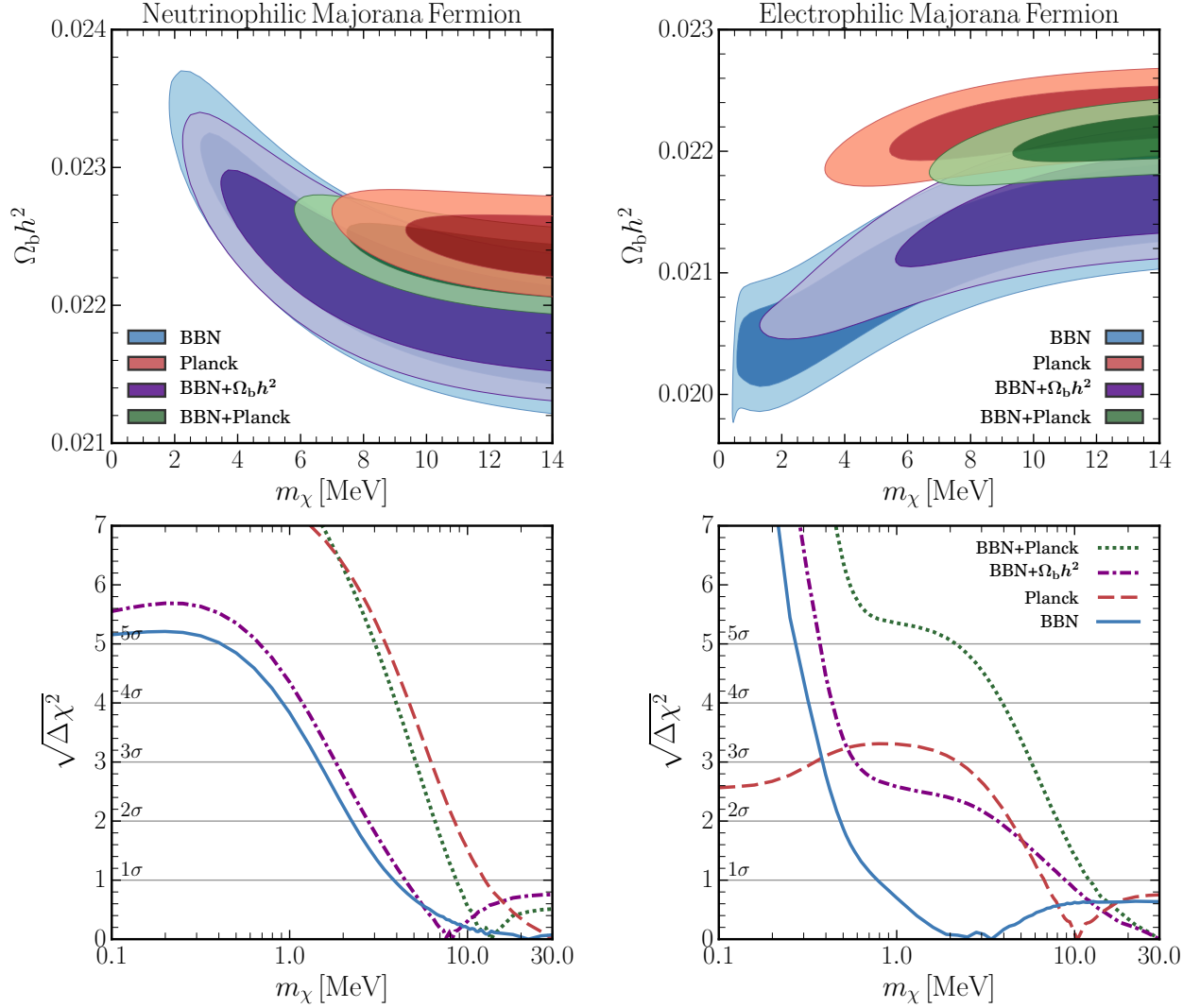
FIG. 2. *Upper Panels:* Contour plots showing the 1σ and 2σ confidence intervals in the $(\Omega_{\rm b}h^2, m_\chi)$ plane for a Majorana fermion with mass m_χ in thermal equilibrium with the SM plasma. *Lower Panels:* Marginalized $\Delta\chi^2$ as a function of m_χ. Solid lines correspond to BBN, dashed to Planck CMB 2018 observations, dash-dotted to the combination BBN+$\Omega_{\rm b}h^2$ and dotted to BBN+Planck. The *left/right panel* corresponds to neutrinophilic/electrophilic particles.

In order to illustrate the extent to which cosmological observations constrain the masses of light thermally coupled BSM species, we depict in the upper frames of Figure 2 the 1σ and 2σ confidence intervals in the $(\Omega_{\rm b}h^2, m_\chi)$ plane for our four baseline analyses for the case of a Majorana fermion. We observe degeneracies between $\Omega_{\rm b}h^2$ and m_χ in some regions of parameter space for the BBN analysis, but thanks to the precision with which the primordial element abundances are measured and the CMB is observed, a lower bound on m_χ can be set. From the lower panels of Figure 2 we see that neutrinophilic BSM states with $m_\chi \lesssim 1$ MeV are strongly disfavoured by BBN. In the case of electrophilic states, the same holds, albeit for relatively lighter BSM particles with $m_\chi \lesssim 0.3$ MeV. These results show that current cosmological observations set very stringent constraints on light species in thermal equilibrium during the time of BBN. In addition, the constraints derived from BBN are independent of the assumed cosmological model. In particular, BBN disfavours thermal particles with $m_\chi < 0.1$ MeV at more than 5σ – with the sole exception of a neutrinophilic neutral scalar that is disfavoured at 3.3σ. This is done only by using the observed values of $Y_{\rm P}$ and D/H$|_{\rm P}$. The reader is referred to Figure 9 in Appendix D for the $\Delta\chi^2(m_\chi)$ of each scenario considered in this study.

Type	BSM Particle		Current Constraints					Forecasted Constraints	
	Particle	g-Spin	BBN	BBN+$\Omega_b h^2$	Planck	Planck+H_0	BBN+Planck	Simons Obs.	CMB-S4
Neutrinophilic	Majorana	2-F	2.2	2.8	8.4	4.9	6.6	12.5	13.5
	Dirac	4-F	3.7	5.4	11.3	8.0	9.4	15.3	16.2
	Scalar	1-B	1.2	1.3	5.6	1.6	3.7	9.8	10.7
	Complex Scalar	2-B	2.3	2.9	8.5	5.1	6.7	12.5	13.5
	Vector	3-B	3.1	4.4	10.1	6.8	8.3	14.1	15.1
Electrophilic	Majorana	2-F	0.5	3.7	4.4	9.2	8.0	12.2	13.2
	Dirac	4-F	0.7	7.0	7.4	12.0	10.9	14.9	15.9
	Scalar	1-B	0.4	0.6	2.4*	6.4	5.2	9.4	10.5
	Complex Scalar	2-B	0.5	4.0	4.6	9.2	8.1	12.2	13.2
	Vector	3-B	0.6	5.8	6.3	10.9	9.8	13.8	14.8

TABLE II. Lower bounds at 95.4% CL on the masses of various thermal BSM particles in MeV. The columns correspond to constraints using data from various sources as detailed in Sections III and VI for current and forecasted constraints respectively. The rows correspond to BSM particles with a different number of internal degrees of freedom g and spin (F: fermion, B: boson). The upper/lower parts of the table correspond to purely neutrinophilic/electrophilic particles. *This bound is only at 86% CL.

BBN and BBN+$\Omega_b h^2$

From Table II we observe that from the current determinations of the primordial helium and deuterium abundances (BBN) alone we are able to place a lower bound on the mass of $m_\chi > 0.4$ MeV at 95.4% CL. This bound is independent of the spin, number of internal degrees of freedom of the species at hand and also of whether the particle interacts only with neutrinos or electrons/photons. We notice that the bounds for neutrinophilic species, $m_\chi > (1.2 - 3.7)$ MeV, are stronger as compared with the bounds for electrophilic species, $m_\chi > (0.4 - 0.7)$ MeV. When very conservative information about the value of $\Omega_b h^2$ from CMB observations is included (BBN+$\Omega_b h^2$), the bounds get slightly stronger to the level of $m_\chi > (1.3-4.4)$ MeV for neutrinophilic species and $m_\chi > (0.6-7.0)$ MeV for electrophilic ones.

Planck

From the Planck column in Table II one can clearly see that Planck typically sets more restrictive constraints than BBN. For neutrinophilic relics $m_\chi > (5.6 - 11.3)$ MeV, while for electrophilic relics $m_\chi > (4.4 - 7.4)$ MeV. The sole exception to this is an electrophilic scalar boson that cannot be constrained at 2σ from Planck CMB observations (as can be seen from Figure 1). Nonetheless, we find that a lower bound of $m_\chi > 2.4$ MeV at 86% CL can still be set.

Planck+H_0

Planck constraints are based solely on CMB observations. However, the actual value of N_{eff} may be different if local determinations of the Hubble constant are taken into account as discussed in Section III. We find that when local measurements of H_0, BAO data and Planck CMB observations are considered, the bounds for neutrinophilic relics are relaxed as compared to Planck data alone, while the bounds for electrophilic relics become stronger. This is because the inclusion of the local determination of H_0 results in a higher mean value of N_{eff}, which leads to a preference for neutrinophilic relics that generally contribute to $N_{eff} > N_{eff}^{SM}$. Still, this data combination rules out thermal BSM particles of $m_\chi > 1.6$ MeV at 95.4% CL.

BBN+Planck

Finally, when Y_P and D/H|$_P$ data are combined with Planck CMB observations we find that the constraints for neutrinophilic species are slightly relaxed as compared to Planck alone, yielding $m_\chi > (3.7 - 9.4)$ MeV, while the bounds get stronger for electrophilic relics, yielding $m_\chi > (5.2 - 10.9)$ MeV. This is a mere result of a slight $\sim 0.9\sigma$ tension between the $\Omega_b h^2$ that is inferred from BBN and CMB observations [105]. Note that from the lower panels of Figure 2, Plank+BBN data strongly disfavours very light BSM thermal species.

Summary

We have set strong constraints from a combination of cosmological measurements, including the primordial helium and deuterium abundances and CMB observations by the Planck satellite. For the combination of BBN+Planck data, we find that the mass of purely electrophilic and neutrinophilic BSM species in thermal equilibrium with the SM plasma – independently of their spin and number of degrees of freedom – should satisfy $m_\chi > 3.7$ MeV at 95.4% CL.

V Current Cosmological Constraints on Generic WIMPs

Up to this point we have restricted our analysis to particles that interact solely with neutrinos or electrons/photons. In this section, we explore the cosmological constraints that can be placed on particles which interact with both neutrinos and electrons. First, we provide a brief overview of the phenomenology of this scenario and then we describe the constraints we find on such particles from BBN and CMB observations. The reader is referred to Table VI for a suite of constraints on thermal WIMPs that annihilate at a different rate to electrons/photons and neutrinos, to Table III for lower bounds on the neutrino decoupling temperature $T_\nu^{\rm dec}$, and to Figure 3 for the cosmological implications of a non-standard $T_\nu^{\rm dec}$.

V.1 Overview of Cosmological Implications

The key consequence of BSM particles in thermal equilibrium with the SM plasma through interactions with both electrons and neutrinos is that they efficiently act as to delay the process of neutrino decoupling. A reduction of the neutrino decoupling temperature as compared to the SM case, $T_\nu^{\rm dec}|_{\rm SM}$, implies that:

- The entropy released by electron-positron annihilation at $T \lesssim m_e$ is shared among both photons and neutrinos, yielding $T_\nu > T_\nu^{\rm SM}$ and $T_\gamma < T_\gamma^{\rm SM}$ and therefore implying $N_{\rm eff} > N_{\rm eff}^{\rm SM}$.
- The number density of baryons is enhanced as compared with the SM case, as a result of the smaller number density of photons after electron-positron annihilation.
- A higher expansion rate of the Universe for $T \lesssim m_e$.

Both stable and unstable particles can efficiently delay the process of neutrino decoupling. For example, in the case of a thermal WIMP that annihilates equally to neutrinos and electrons, the energy will be efficiently transferred between the electromagnetic and neutrino sectors of the plasma as a result of $e^+ e^- \leftrightarrow \chi\chi \leftrightarrow \bar\nu\nu$ processes[6] until $T/m_\chi \sim 1/10$ [103]. If one considers $m_\chi = 2$ MeV, neutrino decoupling will occur at $T_\nu^{\rm dec} \sim 0.2$ MeV and hence at a temperature that is much lower than the SM one of $T_\nu^{\rm dec}|_{\rm SM} \simeq 1.9$ MeV.

Unstable particles that interact with both neutrinos and electrons would delay the process of neutrino decoupling, typically for even smaller temperatures than WIMPs. For example, consider a light $U(1)_{B-L}$ gauge boson Z' that decays at a similar rate to neutrinos and electrons. By comparing the inverse decay rate to the Hubble parameter one can show that via $e^+ e^- \leftrightarrow Z' \leftrightarrow \bar\nu\nu$ interactions the process of neutrino decoupling will be delayed until

$$\frac{m_{Z'}}{T} \simeq \log\left[\frac{\Gamma_{Z'} M_{\rm Pl}}{1.66\,\sqrt{g_\star}\,m_{Z'}^2}\right] + \frac{7}{2}\log\left[\frac{m_{Z'}}{T}\right]\,, \tag{17}$$

where $\Gamma_{Z'} \simeq g_{B-L}^2 m_{Z'}/(4\pi)$ is the decay width of the Z' and g_{B-L} is the gauge coupling of the corresponding $U(1)_{B-L}$ symmetry. Taking representative numbers, we can see that this particle will delay the process of neutrino decoupling until

$$\frac{m_{Z'}}{T} \simeq 30 + \log\left[\left(\frac{g_{B-L}}{10^{-6}}\right)^2 \frac{5\,{\rm MeV}}{m_{Z'}}\right] + \frac{7}{2}\log\left[\frac{m_{Z'}}{30\,T}\right]\,, \tag{18}$$

and hence a Z' with $m_{Z'} \simeq 5$ MeV and $g_{B-L} \simeq 10^{-6}$ will delay neutrino decoupling until $T_\nu^{\rm dec} \sim 0.2$ MeV; a temperature that is one order of magnitude smaller than the SM one.

Temperature of Neutrino Decoupling	Current Constraints					Forecasted Constraints	
	BBN	BBN+$\Omega_{\rm b}h^2$	Planck	Planck+H_0	BBN+Planck	Simons Obs.	CMB-S4
$T_\nu^{\rm dec}$	0.34	0.36	0.65	0.43	0.53	1.0	1.1

TABLE III. Lower bounds at 95.4% CL on the neutrino decoupling temperature in MeV.

---

[6] For regions of parameter space in which $m_\chi < m_e$, it is understood that the annihilation proceeds into $\gamma\gamma$ and not into $e^+ e^-$ by pure kinematics.

V.2 Constraints

In this section we follow two avenues to set constraints on particles that interact with both neutrinos and electrons: *i)* we set constraints on the masses of various types of WIMPs that annihilate with a thermal cross-section, but with varying final state annihilation ratios to electrons and neutrinos, and *ii)* we set constraints on the neutrino decoupling temperature T_ν^{dec} that can be mapped into many extensions of the SM with light interacting species.

We consider all possible combinations of spins and final state annihilation ratios of electrons to neutrinos, ranging from $e : \nu = 10^6 : 1$ to $e : \nu = 1 : 10^6$. All the resulting lower bounds of the WIMP mass at 95.4% CL can be found in Table VI (see Table IV for the particular case of a Majorana dark matter fermion). The three main conclusions that can be inferred from this analysis are:

- Current BBN observations bound the thermal dark matter mass to be $m_\chi > 0.4\,\mathrm{MeV}$ at 2σ. This can be seen from Table VI. This constraint is independent of the spin or the number of internal degrees of freedom of the given WIMP, as well as of the annihilation channel to SM species.

- For any $e : \nu$ annihilation ratio and given type of WIMP, with the exception of a neutral scalar particle, Planck CMB observations set a 2σ lower bound on m_χ. Similarly, Planck+BBN bound set $m_\chi > 0.8\,\mathrm{MeV}$ a 2σ. These bounds are independent upon the spin of the particle and whether the annihilation is s-wave or p-wave.

- WIMPs with an annihilation ratio $e : \nu \sim 10^4 : 1$ are particularly elusive to BBN and CMB observations; only BSM particles of $m_\chi \lesssim 1.3\,\mathrm{MeV}$ can be constrained at present. This results from the fact that on one hand, such species preferably dump entropy into the electromagnetic sector of the plasma, while on the other hand, delayed neutrino decoupling causes that entropy to be shared with neutrinos. This yields $N_{\mathrm{eff}} \simeq N_{\mathrm{eff}}^{\mathrm{SM}}$.

In addition, we set a lower bound on the temperature at which neutrinos decouple. In order to do so, we do not include any BSM species in the evolution, but solve for neutrino decoupling as in the Standard Model but with a modified Fermi constant G_{F}' in the neutrino-electron rates as in Equation (6), such that the temperature of neutrino decoupling is altered with respect to the SM, $T_\nu^{\mathrm{dec}} = 1.9\,\mathrm{MeV}\,(G_{\mathrm{F}}/G_{\mathrm{F}}')^{2/3}$. For this computation we neglect the electron mass and evaluate the relevant χ^2 on a grid of $(T_\nu^{\mathrm{dec}}, \Omega_{\mathrm{b}}h^2)$. The results of such analysis are presented in Table III.

We find that $T_\nu^{\mathrm{dec}} > 0.34\,\mathrm{MeV}$ at 95.4% CL from BBN observations. Planck CMB observations are more stringent than BBN and set $T_\nu^{\mathrm{dec}} > (0.43 - 0.65)\,\mathrm{MeV}$ depending on whether local measurements of H_0 are included or not. In addition, from the right panel of Figure 3, we can appreciate that $T_\nu^{\mathrm{dec}} \lesssim 0.2\,\mathrm{MeV}$ are highly disfavoured by current
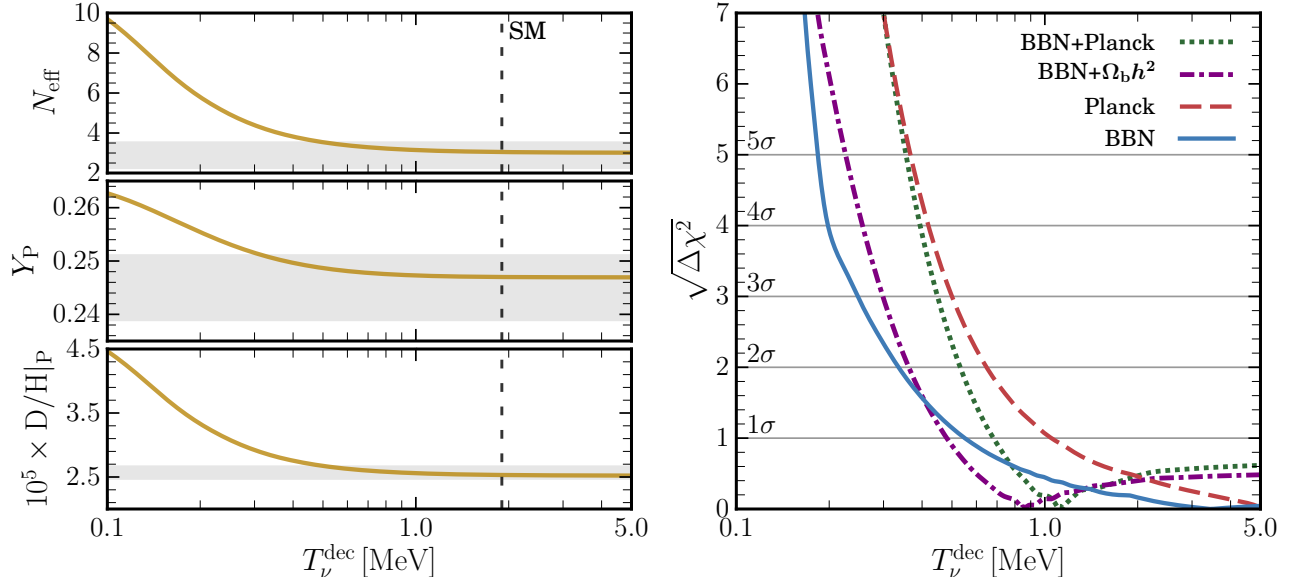

FIG. 3. *Left panels:* Impact of a non-standard neutrino decoupling temperature on the cosmological observables N_{eff}, Y_{P} and D/H|$_{\mathrm{P}}$. The Y_{P} and D/H|$_{\mathrm{P}}$ predictions are computed with $\Omega_{\mathrm{b}}h^2 = 0.021875$ and $\tau_n = 879.5\,\mathrm{s}$. The grey contours correspond to the mean $\pm 2\sigma$ measurements that enter our BBN and Planck data analysis, see Eqs. (13), (14) and (15). *Right panel:* Marginalized $\Delta\chi^2$ as a function of the neutrino decoupling temperature. Solid lines correspond to BBN constraints, dashed to Planck CMB observations, dash-dotted to the combination BBN+$\Omega_{\mathrm{b}}h^2$ and dotted to BBN+Planck.

Type	Probe	$e : \nu$ Annihilation Ratio											
		$1{:}10^6$	$1{:}10^5$	$1{:}10^4$	$1{:}10^3$	$1{:}10^2$	$1{:}10^1$	$1{:}1$	$10^1{:}1$	$10^2{:}1$	$10^3{:}1$	$10^4{:}1$	$10^5{:}1$	$10^6{:}1$
Majorana	BBN	2.2	2.0	1.8	1.8	2.0	2.3	2.4	2.2	1.9	1.6	1.1	0.7	0.5
	BBN+$\Omega_b h^2$	2.6	2.2	1.8	1.9	2.1	2.4	2.6	2.3	1.9	1.5	1.1	0.9	3.3
	Planck	8.2	7.6	4.6	3.4	3.6	4.1	4.5	3.8	3.0	2.1	1.1	0.3	4.1
	Planck+H_0	4.7	3.3	2.0	2.0	2.3	2.7	3.0	3.2	2.5	1.8	0.9	0.2; 0.4 - 8.4	8.9
	BBN+Planck	6.4	5.4	3.1	2.7	2.9	3.4	3.7	3.2	2.6	1.9	1.1	7.0	7.8

TABLE IV. Lower bounds at 95.4% CL on the mass of a Majorana thermal dark matter particle in MeV. The rows correspond to constraints using data from various sources as detailed in Section III. The columns correspond to the annihilation ratio between electrons/photons and neutrinos in the final state. Here we have assumed $\langle \sigma v \rangle = \langle \sigma v \rangle_{\text{WIMP}}$.

cosmological observations. Finally, joint BBN+Planck CMB observations constrain $T_\nu^{\text{dec}} > 0.63\,\text{MeV}$ and we expect next generation of CMB observations to be able to test $T_\nu^{\text{dec}} \lesssim 1\,\text{MeV}$.

The bound on the neutrino decoupling temperature is generic and can be directly mapped into a constraint on the mass and couplings of various BSM species interacting both with neutrinos and electrons. The phenomenology of such type of scenarios has been studied in detail in the context of a very light $U(1)_{\mu-\tau}$ gauge boson [83], but from Equation (18) we can directly map a bound on $T_\nu^{\text{dec}} > 0.3\,\text{MeV}$ into a constraint on other scenarios. For example, by considering the conservative bound $T_\nu^{\text{dec}} > 0.3\,\text{MeV}$ in the case of a light $U(1)_{B-L}$ gauge boson, from Equation (18) we can appreciate that gauge bosons of $m_{Z'} \lesssim 10$ MeV with $g_{B-L} \gtrsim 5 \times 10^{-7}\sqrt{10\,\text{MeV}/m_{Z'}}$ are excluded by cosmological observations. Note that this constraint is independent of the branching fraction of such Z' to invisible particles.

VI Future Cosmological Constraints

VI.1 Cosmic Microwave Background

There are a number of proposed future CMB experiments that would provide an accurate determination of the relevant cosmological parameters for this study: $\Omega_b h^2$, N_{eff}, Y_P. Proposed experiments include satellite missions like PICO [131] or CORE [132] and ground-based experiments like the Simons Observatory [133], CMB-S4 [134, 135] and CMB-HD [136]. In this section we consider the reach of the Simons Observatory[7], because it is fully funded and expected to deliver measurements within the next few years, and that of CMB-S4[8], because it aims to reach a sub-percent determination of N_{eff}.

We use the Fisher Matrix method to forecast the reach of CMB-S4 (see Appendix F for details) and use the baseline covariance matrix from the Simons Observatory collaboration. In analogy with (14), the relevant parameters read:

$$
\begin{aligned}
&\textit{Simons Observatory} && \textit{CMB-S4} \\
&(\Omega_b h^2,\, N_{\text{eff}},\, Y_P)|_{\text{Fiducial}} = (0.022360,\, 3.046,\, 0.2472), && (\Omega_b h^2,\, N_{\text{eff}},\, Y_P)|_{\text{Fiducial}} = (0.022360,\, 3.046,\, 0.2472), \\
&(\sigma_1,\, \sigma_2,\, \sigma_3) = (0.000073,\ \ 0.11,\, 0.0066), && (\sigma_1,\, \sigma_2,\, \sigma_3) = (0.000047,\, 0.081,\, 0.0043), \\
&(\rho_{12},\, \rho_{13},\, \rho_{23}) = (0.072,\, 0.33,\, -0.86), && (\rho_{12},\, \rho_{13},\, \rho_{23}) = (0.25,\, 0.22,\, -0.84),
\end{aligned}
$$

Note that the forecasted errors on N_{eff} look substantially larger than what is typically quoted in the literature and this is simply a result of the fact we also allow Y_P to vary.

Figure 4 shows the reach of future CMB observations to m_χ and $\Omega_b h^2$ for a Majorana fermion. From Table I, we notice that future CMB experiments will be able to probe substantially heavier BSM states than current CMB observations. In particular, the Simons Observatory is expected to set a lower bound on the mass of light BSM species of $m_\chi > 9.4$ MeV, while CMB-S4 is expected to extend this bound to $m_\chi > 10.5$ MeV, both at 95.4% CL.

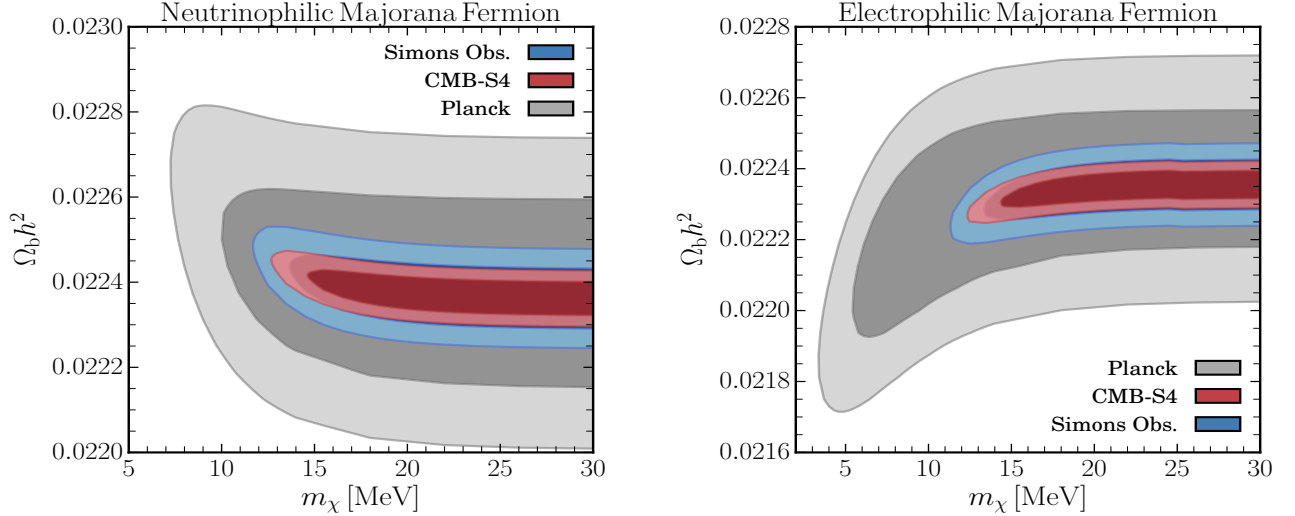[7] https://simonsobservatory.org/.
[8] https://cmb-s4.org/.

FIG. 4. Contour plots showing the current and forecasted 1σ and 2σ confidence intervals in the $(\Omega_b h^2, m_\chi)$ plane for a BSM Majorana fermion in thermal equilibrium with the SM plasma during BBN. The grey contours correspond to current constraints by Planck 2018, while the blue and red contours correspond to the expected reach of the Simons Observatory and CMB-S4 experiments respectively. *Left*: Neutrinophilic. *Right*: Electrophilic.

VI.2 Big Bang Nucleosynthesis

Forecasting the reach of future determinations of the light primordial element abundances is not straightforward. However, from an observational perspective, the precision with which the primordial deuterium abundance is measured, is expected to improve by an order of magnitude with upcoming 30 m telescope facilities [114, 137]. From a theoretical perspective, the nuclear reaction rates that significantly contribute to the error budget in the theoretical prediction of $D/H|_P$ are expected to be measured with higher accuracy by the LUNA collaboration [138]. It is therefore feasible that, in the near future, a per mille determination of $D/H|_P$ could be achieved. Regarding Y_P, while the situation is much less clear, it is still conceivable that Y_P could be narrowed down with greater than 1% accuracy in the future [137].

In order to account for many possible future scenarios, and in a similar spirit to [139], we estimate the reach of future measurements of Y_P and $D/H|_P$ to the mass of thermal BSM state by assuming that the measured values of Y_P and $D/H|_P$ correspond to the values as predicted by PRIMAT using $\Omega_b h^2 = 0.02236$ and $\tau_n = 879.5$ s – namely, $Y_P = 0.2472$ and $D/H|_P = 2.439 \times 10^{-5}$ – and by varying the joint theoretical + observational accuracy with which they are determined.

In Figure 5, we show the forecasted 2σ lower bounds on the mass of a Majorana fermion in thermal equilibrium with the SM plasma as a function of the fractional error in Y_P and $D/H|_P$. It is clear that the bounds are largely driven by helium measurements, while $D/H|_P$ measurements are instead expected to provide accurate determinations of $\Omega_b h^2$. As such, if a prior for $\Omega_b h^2$ is provided from CMB observations, then $D/H|_P$ measurements do play an important role in constraining light BSM species in thermal equilibrium with the SM plasma.

VII   Discussion

In this section we comment on some of the implications of the constraints on thermal BSM species derived in this work. In particular, we discuss examples of theoretical scenarios in which these bounds are relevant, how the bounds are altered when additional BSM states are present and the robustness of our constraints with respect to non-standard expansion histories of the Universe. Finally, we provide a brief comparison with recent literature.

VII.1 Particle Physics Scenarios

Our constraints on thermally coupled BSM species apply to various particle physics models, typically within the context of thermal dark matter. The bounds outlined in Table II apply to both s-wave and p-wave annihilating
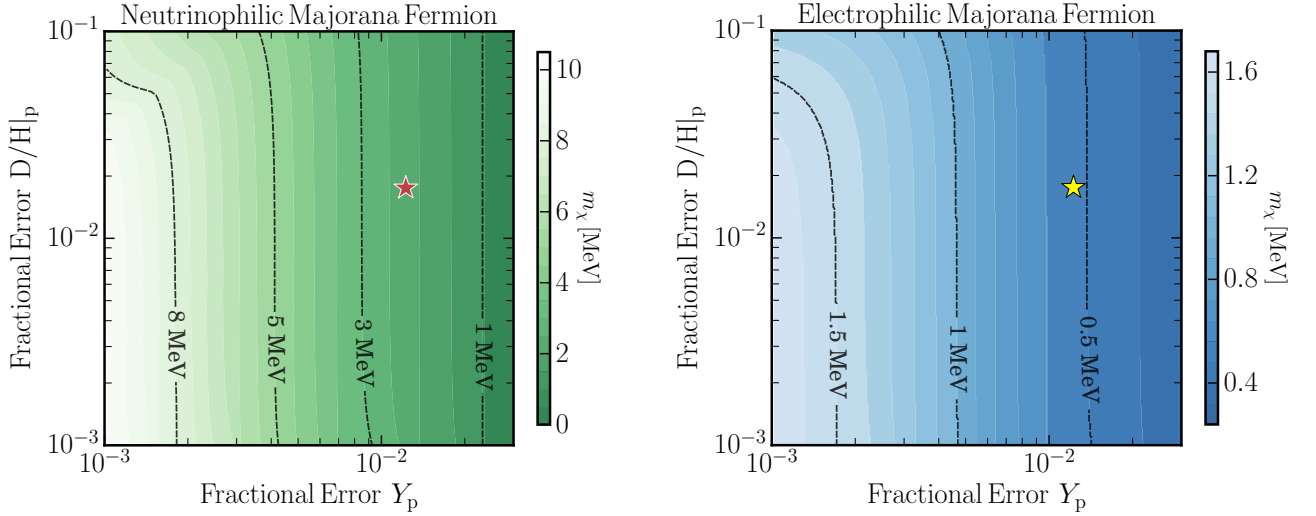
FIG. 5. Projected 2σ exclusion limits for the mass of a Majorana BSM particle in thermal equilibrium during BBN. Bounds are shown as a function of the fractional errors (joint theoretical and observational) in the primordial helium and deuterium abundances. The red and yellow stars correspond to the current precision. *Left*: Neutrinophilic. *Right*: Electrophilic.

thermal relics. Such bounds are particularly relevant for s-wave and p-wave dark matter particles annihilating to neutrinos [21–25], since they are difficult to test at neutrino experiments [55–59]. In addition, these bounds will be relevant for p-wave annihilating relics to electrons and positrons, as in the case of Majorana/Dirac dark matter annihilating via dark photon/Higgs exchange [15–17, 28]. Furthermore, the bounds apply to species that need not to be the entirety of the dark matter, see e.g. [79], and have also been applied to scenarios in which dark matter particles interact with quarks [140].

The bounds derived for BSM species that annihilate into electrons and neutrinos with different ratios are, for instance, relevant for scenarios involving a gauging of SM global symmetries such as $U(1)_{L_\mu - L_\tau}$ [32, 141, 142] or $U(1)_{B-L}$ [143, 144]. Finally, these bounds also apply to asymmetric dark matter sectors interacting with SM species [145, 146]. Asymmetric dark matter set-ups require annihilation cross sections that are larger than for WIMPs, and as such thermal equilibrium in the early Universe is realised. Note, however, that these bounds do not apply to scenarios in which the given BSM species is never brought into thermal equilibrium, as in the case of freeze-in [34, 37], or simply for significantly smaller couplings than those outlined in Equations (2) and (3) [147]. For slightly smaller couplings than those in Equations (2) and (3), BBN can still serve as a useful probe [148].

The bounds presented in this study do not only apply to dark matter particles, but also to unstable mediators. For example, the bounds constrain relevant parameter spaces for various neutrinophilic scalars and vector bosons, regardless of whether they are related to dark matter [27, 56] or not [149]. Similarly, light dark Higgses or dark photons are also constrained. The constraints are particularly relevant for dark photons that decay into hidden sector species. Specifically, the bounds rule out MeV-scale dark photons that decay invisibly for kinetic mixing parameters in the range $10^{-7} \lesssim \epsilon \lesssim 10^{-5}$. This region of parameter space is mildly constrained from colliders, beam dump experiments and supernova cooling [73, 150, 151].

VII.2 Modified Cosmological Histories

The bounds derived above were obtained assuming that only one particle alters the usual SM picture of a radiation dominated Universe between neutrino decoupling and recombination. Here we comment on how we expect the constraints to be altered when additional BSM species are present or non-standard thermal histories are considered.

Typically, dark matter particles are accompanied with mediators of similar mass. The presence of two (or more) neutrinophilic/electrophilic particles in thermal equilibrium in the early Universe would result in stronger bounds on the individual masses of the particles as compared to those outlined in Table II. Another very plausible contribution to the energy density in the Universe during BBN and recombination is massless dark radiation adding to ΔN_{eff}. Massless dark radiation will contribute to the expansion rate of the Universe and hence lead to an enhancement of Y_P with respect to the SM prediction [90–92]. This is precisely the same effect as the light BSM particles we consider (see middle panels of Figure 1) and hence the BBN bounds should simply strengthen in such a scenario.

The CMB constraints on the other hand, will be relaxed in the case of electrophilic particles [152] but strengthen for neutrinophilic species. Similarly, perhaps a more exotic non-negligible primordial leptonic asymmetry could be present and modify nucleosynthesis and N_{eff} as relevant for CMB observations [106]. In such a scenario, we expect the bounds presented here to be modified [153] but not substantially given the accuracy with which N_{eff} and the helium and deuterium abundances have now been measured.

One of the key assumptions to derive the bounds in this study was that the particles we consider must have been in thermal equilibrium. Since we know from both BBN and CMB observations that the Universe should have at least reached a temperature of $T > 1.8\,\text{MeV}$ [154, 155], the particles we consider will indeed have reached thermal equilibrium.

Another assumption in order to derive these bounds is that the baryon-to-photon ratio remains constant between the end of BBN and recombination. This is well justified on the basis that late time electromagnetic energy injections are strongly constrained by BBN [156–158] and CMB spectral distortions [159, 160].

VII.3 Comparison with Previous Literature

The cosmological implications of MeV-scale thermal dark matter particles were highlighted a while ago in [94]. Since then, a number of groups [94–103] have used BBN and/or CMB observations to set constraints on the masses and properties of various thermally coupled species in the early Universe.

One of the main differences between previous studies and the one presented here is the accuracy with which the primordial element abundances have been calculated. In particular, we account for non-instantaneous neutrino decoupling in the presence of light BSM particles [103, 104] and we use the state-of-the-art BBN code `PRIMAT` [105]. With respect to previous CMB analyses, we find very similar results to those presented in [103] that accounted for the same effects and used Planck 2018 data. Regarding BBN constraints, we can differentiate between two types of studies: some that fixed the baryon-to-photon ratio to be the best-fit from CMB observations at the time [95, 96, 99, 102], while others allowed $\Omega_{\text{b}} h^2$ to vary and then fitted it to measurements of Y_{P} and $\text{D/H}|_{\text{P}}$ simultaneously with m_χ [97, 98, 101]. In this work, we marginalize over all possible values of $\Omega_{\text{b}} h^2$. The comparison with each reference goes as follows: firstly, when comparing with [97], we find that the constraints presented in this work on purely electrophilic BSM states are a factor $1.5 - 2.5$ more stringent. Secondly, a direct comparison with [98] is not possible since there are no bounds reported from a BBN only analysis. Thirdly, [101] did not found a BBN bound for a real neutrinophilic scalar boson at 95.4% CL while we find $m_\chi > 1.2\,\text{MeV}$ at such CL. We believe that these differences with previous studies are largely driven by the use of more recent and precise determinations of Y_{P} and $\text{D/H}|_{\text{P}}$.

Finally, our work represents the first exhaustive study of WIMPs that annihilate differently to both electrons and neutrinos. Furthermore, we provide bounds on the temperature at which neutrinos decouple that can be mapped into various relevant particle physics scenarios.

VIII   Conclusions

MeV-scale BSM species in thermal equilibrium with the Standard Model plasma during Big Bang Nucleosynthesis have important cosmological consequences, as can be seen from Figure 1. In this work, we have analyzed in detail and with precision the impact of such states on the synthesis of the primordial element abundances and CMB observations. To this end, we have modelled the early Universe evolution using the methods of [103, 104] and by modifying the state-of-the-art BBN code `PRIMAT` [105]. We have used a suite of cosmological observations, as summarized in Table I, to set constraints on the masses of various types of BSM states in thermal equilibrium with the SM plasma during BBN. We summarize the derived constraints in Table II for purely electrophilic and neutrinophilic BSM states. In Tables IV and VI we consider WIMPs that have different annihilation ratios to SM species. Finally, in Table III we outline the lower bound on a non-standard neutrino decoupling temperature. The main conclusions that can be drawn from this study are:

- BBN observations set a lower bound on electrophilic/neutrinophilic thermal species of $m_\chi > 0.4/1.2\,\text{MeV}$ at 95.4% CL. This bound is independent of the spin and the number of internal degrees of freedom of the species at hand. In particular, any WIMP, irrespective of its annihilation being s-wave or p-wave and the annihilation final state, is bounded to have $m_\chi > 0.4\,\text{MeV}$ at 95.4% CL.

- Very light ($m_\chi < 0.1\,\text{MeV}$) thermal relics are highly disfavoured by current measurements of the primordial light elements (at more than 5σ). The sole exception to this rule is a purely neutrinophilic neutral scalar state, which is nonetheless ruled out at 3.3σ.

- BBN and CMB observations jointly constrain neutrinophilic and electrophilic thermal BSM states to have a mass $m_\chi > 3.7\,\mathrm{MeV}$ at 95.4% CL. This bound is independent of the spin or internal degrees of freedom of the given species and applies to both s-wave and p-wave annihilating dark matter relics, as well as to unstable dark sector mediators. Table II summarizes the constraints for various BSM states.

- We argue that the bounds presented in this study are expected to be strengthened in the presence of additional species beyond those considered here. In addition, bounds based on BBN are largely insensitive to modifications of the assumed cosmological model.

- We have set constraints on BSM particles with masses $m_\chi \lesssim 20\,\mathrm{MeV}$ that interact with both electrons and neutrinos. Such states efficiently delay the process of neutrino decoupling, which allows BBN to constrain the temperature of neutrino decoupling to be $T_\nu^{\mathrm{dec}} > 0.34\,\mathrm{MeV}$ at 95.4% CL. Moreover, we find that decoupling temperatures $T_\nu^{\mathrm{dec}} < 0.2\,\mathrm{MeV}$ are highly disfavoured ($> 5\sigma$) by BBN and/or CMB observations.

- Future CMB experiments such as the Simons Observatory [133] and CMB-S4 [134, 135], will constrain generic thermal BSM particles of $m_\chi \lesssim (10-15)\,\mathrm{MeV}$. Similarly, we highlighted the impact of future primordial helium and deuterium determinations to light BSM states in thermal equilibrium with the SM plasma during nucleosynthesis.

To summarize, cosmology strongly constrains new physics at the MeV scale. Cosmological constraints are competitive with and complementary to those from colliders, beam dump and neutrino experiments, (in)direct dark matter searches, as well as from astrophysical probes.

Acknowledgments

[1] ATLAS collaboration, M. Aaboud et al., *Search for dark matter and other new phenomena in events with an energetic jet and large missing transverse momentum using the ATLAS detector*, *JHEP* **01** (2018) 126 [`1711.03301`].

[2] CMS collaboration, A. M. Sirunyan et al., *Search for narrow and broad dijet resonances in proton-proton collisions at* $\sqrt{s} = 13$ *TeV and constraints on dark matter mediators and other new particles*, *JHEP* **08** (2018) 130 [`1806.00843`].

[3] XENON collaboration, E. Aprile et al., *Dark Matter Search Results from a One Ton-Year Exposure of XENON1T*, *Phys. Rev. Lett.* **121** (2018) 111302 [`1805.12562`].

[4] LUX collaboration, D. S. Akerib et al., *Results from a search for dark matter in the complete LUX exposure*, *Phys. Rev. Lett.* **118** (2017) 021303 [`1608.07648`].

[5] PandaX-II collaboration, X. Cui et al., *Dark Matter Results From 54-Ton-Day Exposure of PandaX-II Experiment*, *Phys. Rev. Lett.* **119** (2017) 181302 [`1708.06917`].

[6] Fermi-LAT, DES collaboration, A. Albert et al., *Searching for Dark Matter Annihilation in Recently Discovered Milky Way Satellites with Fermi-LAT*, *Astrophys. J.* **834** (2017) 110 [`1611.03184`].

[7] Planck collaboration, N. Aghanim et al., *Planck 2018 results. VI. Cosmological parameters*, `1807.06209`.

[8] M. Escudero, A. Berlin, D. Hooper and M.-X. Lin, *Toward (Finally!) Ruling Out Z and Higgs Mediated Dark Matter Models*, *JCAP* **1612** (2016) 029 [`1609.09079`].

[9] G. Arcadi, M. Dutra, P. Ghosh, M. Lindner, Y. Mambrini, M. Pierre et al., *The waning of the WIMP? A review of models, searches, and constraints*, *Eur. Phys. J.* **C78** (2018) 203 [`1703.07364`].

[10] L. Roszkowski, E. M. Sessolo and S. Trojanowski, *WIMP dark matter candidates and searches?current status and future prospects*, *Rept. Prog. Phys.* **81** (2018) 066201 [`1707.06277`].

[11] GAMBIT collaboration, P. Athron et al., *Status of the scalar singlet dark matter model*, *Eur. Phys. J.* **C77** (2017) 568 [`1705.07931`].

[12] G. Arcadi, A. Djouadi and M. Raidal, *Dark Matter through the Higgs portal*, `1903.03616`.

[13] C. Blanco, M. Escudero, D. Hooper and S. J. Witte, *Z′ Mediated WIMPs: Dead, Dying, or Soon to be Detected?*, `1907.05893`.

[14] R. Essig et al., *Working Group Report: New Light Weakly Coupled Particles*, 2013, `1311.0029`.

[15] J. Alexander et al., *Dark Sectors 2016 Workshop*, 2016, `1608.08632`.

[16] M. Battaglieri et al., *US Cosmic Visions: New Ideas in Dark Matter 2017: Community Report*, 2017, `1707.04591`.

[17] J. Beacham et al., *Physics Beyond Colliders at CERN: Beyond the Standard Model Working Group Report*, `1901.09966`.

[18] C. Boehm and P. Fayet, *Scalar dark matter candidates*, *Nucl. Phys.* **B683** (2004) 219 [`hep-ph/0305261`].

[19] C. Boehm, D. Hooper, J. Silk, M. Casse and J. Paul, *MeV dark matter: Has it been detected?*, *Phys. Rev. Lett.* **92** (2004) 101301 [`astro-ph/0309686`].

[20] J. L. Feng and J. Kumar, *The WIMPless Miracle: Dark-Matter Particles without Weak-Scale Masses or Weak Interactions*, *Phys. Rev. Lett.* **101** (2008) 231301 [`0803.4196`].

[21] C. Boehm, Y. Farzan, T. Hambye, S. Palomares-Ruiz and S. Pascoli, *Is it possible to explain neutrino masses with scalar dark matter?*, *Phys. Rev.* **D77** (2008) 043516 [`hep-ph/0612228`].

[22] Y. Farzan, *A Minimal model linking two great mysteries: neutrino mass and dark matter*, *Phys. Rev.* **D80** (2009) 073009 [`0908.3729`].

[23] Y. Farzan, *Flavoring Monochromatic Neutrino Flux from Dark Matter Annihilation*, *JHEP* **02** (2012) 091 [`1111.1063`].

[24] B. Batell, T. Han, D. McKeen and B. Shams Es Haghi, *Thermal Dark Matter Through the Dirac Neutrino Portal*, *Phys. Rev.* **D97** (2018) 075016 [`1709.07001`].

[25] P. Ballett, M. Hostert and S. Pascoli, *Neutrino Masses from a Dark Neutrino Sector below the Electroweak Scale*, *Phys. Rev.* **D99** (2019) 091701 [`1903.07590`].

[26] J. M. Lamprea, E. Peinado, S. Smolenski and J. Wudka, *Strongly Interacting Neutrino Portal Dark Matter*, `1906.02340`.

[27] M. Blennow, E. Fernandez-Martinez, A. Olivares-Del Campo, S. Pascoli, S. Rosauro-Alcaraz and A. V. Titov, *Neutrino Portals to Dark Matter*, *Eur. Phys. J.* **C79** (2019) 555 [`1903.00006`].

[28] G. Krnjaic, *Probing Light Thermal Dark-Matter With a Higgs Portal Mediator*, *Phys. Rev.* **D94** (2016) 073009 [`1512.04119`].

[29] K. Bondarenko, A. Boyarsky, T. Bringmann, M. Hufnagel, K. Schmidt-Hoberg and A. Sokolenko, *Direct detection and complementary constraints for sub-GeV dark matter*, `1909.08632`.

[30] Y. Hochberg, E. Kuflik, T. Volansky and J. G. Wacker, *Mechanism for Thermal Relic Dark Matter of Strongly Interacting Massive Particles*, *Phys. Rev. Lett.* **113** (2014) 171301 [`1402.5143`].

[31] P. Agrawal, Z. Chacko and C. B. Verhaaren, *Leptophilic Dark Matter and the Anomalous Magnetic Moment of the Muon*, *JHEP* **08** (2014) 147 [`1402.7369`].

[32] A. Kamada, K. Kaneta, K. Yanagi and H.-B. Yu, *Self-interacting dark matter and muon* $g - 2$ *in a gauged* $U(1)_{L_\mu - L_\tau}$ *model*, *JHEP* **06** (2018) 117 [`1805.00651`].

[33] S. Knapen, T. Lin and K. M. Zurek, *Light Dark Matter: Models and Constraints*, *Phys. Rev.* **D96** (2017) 115021 [`1709.07882`].

[34] L. J. Hall, K. Jedamzik, J. March-Russell and S. M. West, *Freeze-In Production of FIMP Dark Matter*, *JHEP* **03** (2010) 080 [`0911.1120`].

[35] X. Chu, T. Hambye and M. H. G. Tytgat, *The Four Basic Ways of Creating Dark Matter Through a Portal*, *JCAP*

1205 (2012) 034 [1112.0493].

[36] T. Hambye, M. H. G. Tytgat, J. Vandecasteele and L. Vanderheyden, *Dark matter from dark photons: a taxonomy of dark matter production*, 1908.09864.

[37] C. Dvorkin, T. Lin and K. Schutz, *Making dark matter out of light: freeze-in from plasma effects*, *Phys. Rev.* **D99** (2019) 115009 [1902.08623].

[38] J. A. Evans, C. Gaidau and J. Shelton, *Leak-in Dark Matter*, 1909.04671.

[39] G. Bertone and M. P. Tait, Tim, *A new era in the search for dark matter*, *Nature* **562** (2018) 51 [1810.01668].

[40] N. Borodatchenkova, D. Choudhury and M. Drees, *Probing MeV dark matter at low-energy e+e- colliders*, *Phys. Rev. Lett.* **96** (2006) 141802 [hep-ph/0510147].

[41] B. Batell, M. Pospelov and A. Ritz, *Probing a Secluded U(1) at B-factories*, *Phys. Rev.* **D79** (2009) 115008 [0903.0363].

[42] P. J. Fox, R. Harnik, J. Kopp and Y. Tsai, *LEP Shines Light on Dark Matter*, *Phys. Rev.* **D84** (2011) 014028 [1103.0240].

[43] R. Essig, J. Mardon, M. Papucci, T. Volansky and Y.-M. Zhong, *Constraining Light Dark Matter with Low-Energy e+e− Colliders*, *JHEP* **11** (2013) 167 [1309.5084].

[44] BABAR collaboration, J. P. Lees et al., *Search for a Dark Photon in e+e− Collisions at BaBar*, *Phys. Rev. Lett.* **113** (2014) 201801 [1406.2980].

[45] KLOE-2 collaboration, A. Anastasi et al., *Search for dark Higgsstrahlung in e+e → μ+μ and missing energy events with the KLOE experiment*, *Phys. Lett.* **B747** (2015) 365 [1501.06795].

[46] BABAR collaboration, J. P. Lees et al., *Search for Invisible Decays of a Dark Photon Produced in e+e− Collisions at BaBar*, *Phys. Rev. Lett.* **119** (2017) 131804 [1702.03327].

[47] LHCB collaboration, R. Aaij et al., *Search for Dark Photons Produced in 13 TeV pp Collisions*, *Phys. Rev. Lett.* **120** (2018) 061801 [1710.02867].

[48] J. D. Bjorken, R. Essig, P. Schuster and N. Toro, *New Fixed-Target Experiments to Search for Dark Gauge Forces*, *Phys. Rev.* **D80** (2009) 075018 [0906.0580].

[49] B. Batell, M. Pospelov and A. Ritz, *Exploring Portals to a Hidden Sector Through Fixed Targets*, *Phys. Rev.* **D80** (2009) 095024 [0906.5614].

[50] S. Andreas, C. Niebuhr and A. Ringwald, *New Limits on Hidden Photons from Past Electron Beam Dumps*, *Phys. Rev.* **D86** (2012) 095019 [1209.6083].

[51] S. Palomares-Ruiz and S. Pascoli, *Testing MeV dark matter with neutrino detectors*, *Phys. Rev.* **D77** (2008) 025025 [0710.5420].

[52] R. Harnik, J. Kopp and P. A. N. Machado, *Exploring nu Signals in Dark Matter Detectors*, *JCAP* **1207** (2012) 026 [1202.6073].

[53] P. deNiverville, D. McKeen and A. Ritz, *Signatures of sub-GeV dark matter beams at neutrino experiments*, *Phys. Rev.* **D86** (2012) 035022 [1205.3499].

[54] B. Batell, P. deNiverville, D. McKeen, M. Pospelov and A. Ritz, *Leptophobic Dark Matter at Neutrino Factories*, *Phys. Rev.* **D90** (2014) 115014 [1405.7049].

[55] N. Klop and S. Ando, *Constraints on MeV dark matter using neutrino detectors and their implication for the 21-cm results*, *Phys. Rev.* **D98** (2018) 103004 [1809.00671].

[56] K. J. Kelly and Y. Zhang, *Mononeutrino at DUNE: New Signals from Neutrinophilic Thermal Dark Matter*, *Phys. Rev.* **D99** (2019) 055034 [1901.01259].

[57] A. Kamada and H.-B. Yu, *Coherent Propagation of PeV Neutrinos and the Dip in the Neutrino Spectrum at IceCube*, *Phys. Rev.* **D92** (2015) 113004 [1504.00711].

[58] C. A. Argelles, A. Kheirandish and A. C. Vincent, *Imaging Galactic Dark Matter with High-Energy Cosmic Neutrinos*, *Phys. Rev. Lett.* **119** (2017) 201801 [1703.00451].

[59] J. B. G. Alvey and M. Fairbairn, *Linking Scalar Dark Matter and Neutrino Masses with IceCube 170922A*, *JCAP* **1907** (2019) 041 [1902.01450].

[60] R. Essig, M. Fernandez-Serra, J. Mardon, A. Soto, T. Volansky and T.-T. Yu, *Direct Detection of sub-GeV Dark Matter with Semiconductor Targets*, *JHEP* **05** (2016) 046 [1509.01598].

[61] S. K. Lee, M. Lisanti, S. Mishra-Sharma and B. R. Safdi, *Modulation Effects in Dark Matter-Electron Scattering Experiments*, *Phys. Rev.* **D92** (2015) 083517 [1508.07361].

[62] S. Derenzo, R. Essig, A. Massari, A. Soto and T.-T. Yu, *Direct Detection of sub-GeV Dark Matter with Scintillating Targets*, *Phys. Rev.* **D96** (2017) 016026 [1607.01009].

[63] R. Essig, T. Volansky and T.-T. Yu, *New Constraints and Prospects for sub-GeV Dark Matter Scattering off Electrons in Xenon*, *Phys. Rev.* **D96** (2017) 043017 [1703.00910].

[64] SUPERCDMS collaboration, R. Agnese et al., *First Dark Matter Constraints from a SuperCDMS Single-Charge Sensitive Detector*, *Phys. Rev. Lett.* **121** (2018) 051301 [1804.10697].

[65] DARKSIDE collaboration, P. Agnes et al., *Constraints on Sub-GeV Dark-MatterElectron Scattering from the DarkSide-50 Experiment*, *Phys. Rev. Lett.* **121** (2018) 111303 [1802.06998].

[66] SENSEI collaboration, O. Abramoff et al., *SENSEI: Direct-Detection Constraints on Sub-GeV Dark Matter from a Shallow Underground Run Using a Prototype Skipper-CCD*, *Phys. Rev. Lett.* **122** (2019) 161801 [1901.10478].

[67] XENON collaboration, E. Aprile et al., *Light Dark Matter Search with Ionization Signals in XENON1T*, 1907.11485.

[68] T. R. Slatyer, *Indirect dark matter signatures in the cosmic dark ages. I. Generalizing the bound on s-wave dark matter annihilation from Planck results*, *Phys. Rev.* **D93** (2016) 023527 [1506.03811].

[69] R. Essig, E. Kuflik, S. D. McDermott, T. Volansky and K. M. Zurek, *Constraining Light Dark Matter with Diffuse*

X-Ray and Gamma-Ray Observations, *JHEP* **11** (2013) 193 [`1309.4091`].

[70] R. Bartels, D. Gaggero and C. Weniger, *Prospects for indirect dark matter searches with MeV photons*, *JCAP* **1705** (2017) 001 [`1703.02546`].

[71] G. G. Raffelt, *Stars as laboratories for fundamental physics*. 1996.

[72] H. K. Dreiner, J.-F. Fortin, C. Hanhart and L. Ubaldi, *Supernova constraints on MeV dark sectors from e^+e^- annihilations*, *Phys. Rev.* **D89** (2014) 105015 [`1310.3826`].

[73] J. H. Chang, R. Essig and S. D. McDermott, *Supernova 1987A Constraints on Sub-GeV Dark Sectors, Millicharged Particles, the QCD Axion, and an Axion-like Particle*, *JHEP* **09** (2018) 051 [`1803.00993`].

[74] W. DeRocco, P. W. Graham, D. Kasen, G. Marques-Tavares and S. Rajendran, *Supernova signals of light dark matter*, `1905.09284`.

[75] Y. Farzan, *Bounds on the coupling of the Majoron to light neutrinos from supernova cooling*, *Phys. Rev.* **D67** (2003) 073015 [`hep-ph/0211375`].

[76] L. Heurtier and Y. Zhang, *Supernova Constraints on Massive (Pseudo)Scalar Coupling to Neutrinos*, *JCAP* **1702** (2017) 042 [`1609.05882`].

[77] W. L. Xu, C. Dvorkin and A. Chael, *Probing sub-GeV Dark Matter-Baryon Scattering with Cosmological Observables*, *Phys. Rev.* **D97** (2018) 103530 [`1802.06788`].

[78] A. Olivares-Del Campo, C. Bhm, S. Palomares-Ruiz and S. Pascoli, *Dark matter-neutrino interactions through the lens of their cosmological implications*, *Phys. Rev.* **D97** (2018) 075039 [`1711.05283`].

[79] A. Berlin, D. Hooper, G. Krnjaic and S. D. McDermott, *Severely Constraining Dark Matter Interpretations of the 21-cm Anomaly*, *Phys. Rev. Lett.* **121** (2018) 011102 [`1803.02804`].

[80] R. J. Wilkinson, C. Boehm and J. Lesgourgues, *Constraining Dark Matter-Neutrino Interactions using the CMB and Large-Scale Structure*, *JCAP* **1405** (2014) 011 [`1401.7597`].

[81] B. Bertoni, S. Ipek, D. McKeen and A. E. Nelson, *Constraints and consequences of reducing small scale structure via large dark matter-neutrino interactions*, *JHEP* **04** (2015) 170 [`1412.3113`].

[82] H. Vogel and J. Redondo, *Dark Radiation constraints on minicharged particles in models with a hidden photon*, *JCAP* **1402** (2014) 029 [`1311.2600`].

[83] M. Escudero, D. Hooper, G. Krnjaic and M. Pierre, *Cosmology with A Very Light L_μ - L_τ Gauge Boson*, *JHEP* **03** (2019) 071 [`1901.02010`].

[84] A. D. Dolgov, S. L. Dubovsky, G. I. Rubtsov and I. I. Tkachev, *Constraints on millicharged particles from Planck data*, *Phys. Rev.* **D88** (2013) 117701 [`1310.2376`].

[85] BELLE-II collaboration, W. Altmannshofer et al., *The Belle II Physics Book*, `1808.10567`.

[86] FASER collaboration, A. Ariga et al., *FASER: ForwArd Search ExpeRiment at the LHC*, `1901.04468`.

[87] S. Alekhin et al., *A facility to Search for Hidden Particles at the CERN SPS: the SHiP physics case*, *Rept. Prog. Phys.* **79** (2016) 124201 [`1504.04855`].

[88] J. P. Chou, D. Curtin and H. J. Lubatti, *New Detectors to Explore the Lifetime Frontier*, *Phys. Lett.* **B767** (2017) 29 [`1606.06298`].

[89] LDMX collaboration, T. kesson et al., *Light Dark Matter eXperiment (LDMX)*, `1808.05219`.

[90] S. Sarkar, *Big bang nucleosynthesis and physics beyond the standard model*, *Rept. Prog. Phys.* **59** (1996) 1493 [`hep-ph/9602260`].

[91] F. Iocco, G. Mangano, G. Miele, O. Pisanti and P. D. Serpico, *Primordial Nucleosynthesis: from precision cosmology to fundamental physics*, *Phys. Rept.* **472** (2009) 1 [`0809.0631`].

[92] M. Pospelov and J. Pradler, *Big Bang Nucleosynthesis as a Probe of New Physics*, *Ann. Rev. Nucl. Part. Sci.* **60** (2010) 539 [`1011.1054`].

[93] PARTICLEDATAGROUP collaboration, M. Tanabashi et al., *Review of Particle Physics*, *Phys. Rev.* **D98** (2018) 030001.

[94] E. W. Kolb, M. S. Turner and T. P. Walker, *The Effect of Interacting Particles on Primordial Nucleosynthesis*, *Phys. Rev.* **D34** (1986) 2197.

[95] P. D. Serpico and G. G. Raffelt, *MeV-mass dark matter and primordial nucleosynthesis*, *Phys. Rev.* **D70** (2004) 043526 [`astro-ph/0403417`].

[96] C. Boehm, M. J. Dolan and C. McCabe, *A Lower Bound on the Mass of Cold Thermal Dark Matter from Planck*, *JCAP* **1308** (2013) 041 [`1303.6270`].

[97] K. M. Nollett and G. Steigman, *BBN And The CMB Constrain Light, Electromagnetically Coupled WIMPs*, *Phys. Rev.* **D89** (2014) 083508 [`1312.5725`].

[98] K. M. Nollett and G. Steigman, *BBN And The CMB Constrain Neutrino Coupled Light WIMPs*, *Phys. Rev.* **D91** (2015) 083505 [`1411.6005`].

[99] C. Boehm, M. J. Dolan and C. McCabe, *Increasing Neff with particles in thermal equilibrium with neutrinos*, *JCAP* **1212** (2012) 027 [`1207.0497`].

[100] C. M. Ho and R. J. Scherrer, *Limits on MeV Dark Matter from the Effective Number of Neutrinos*, *Phys. Rev.* **D87** (2013) 023505 [`1208.4347`].

[101] R. J. Wilkinson, A. C. Vincent, C. Boehm and C. McCabe, *Ruling out the light weakly interacting massive particle explanation of the Galactic 511 keV line*, *Phys. Rev.* **D94** (2016) 103525 [`1602.01114`].

[102] P. F. Depta, M. Hufnagel, K. Schmidt-Hoberg and S. Wild, *BBN constraints on the annihilation of MeV-scale dark matter*, *JCAP* **1904** (2019) 029 [`1901.06944`].

[103] M. Escudero, *Neutrino decoupling beyond the Standard Model: CMB constraints on the Dark Matter mass with a fast and precise $N_{\rm eff}$ evaluation*, *JCAP* **1902** (2019) 007 [`1812.05605`].

[104] M. Escudero, *Neutrino Decoupling Beyond the Standard Model II: Fast and Precise BSM observables in the Early Universe, to appear,* .

[105] C. Pitrou, A. Coc, J.-P. Uzan and E. Vangioni, *Precision big bang nucleosynthesis with improved Helium-4 predictions*, *Phys. Rept.* **754** (2018) 1 [`1801.08023`].

[106] A. D. Dolgov, *Neutrinos in cosmology*, *Phys. Rept.* **370** (2002) 333 [`hep-ph/0202122`].

[107] E. W. Kolb and M. S. Turner, *The Early Universe, Front. Phys.* **69** (1990) 1.

[108] G. Mangano, G. Miele, S. Pastor, T. Pinto, O. Pisanti and P. D. Serpico, *Relic neutrino decoupling including flavor oscillations*, *Nucl. Phys.* **B729** (2005) 221 [`hep-ph/0506164`].

[109] P. F. de Salas and S. Pastor, *Relic neutrino decoupling with flavour oscillations revisited*, *JCAP* **1607** (2016) 051 [`1606.06986`].

[110] G. Steigman, B. Dasgupta and J. F. Beacom, *Precise Relic WIMP Abundance and its Impact on Searches for Dark Matter Annihilation*, *Phys. Rev.* **D86** (2012) 023506 [`1204.3622`].

[111] M. Peimbert, A. Peimbert and V. Luridiana, *A new determination of the primordial helium abundance*, in *Revista Mexicana de Astronomia y Astrofisica Conference Series*, vol. 49 of *Revista Mexicana de Astronomia y Astrofisica, vol. 27*, pp. 181–181, July, 2017.

[112] E. Aver, K. A. Olive and E. D. Skillman, *The effects of He I ?10830 on helium abundance determinations*, *JCAP* **1507** (2015) 011 [`1503.08146`].

[113] Y. I. Izotov, T. X. Thuan and N. G. Guseva, *A new determination of the primordial He abundance using the He i $\lambda 10830$ emission line: cosmological implications*, *Mon. Not. Roy. Astron. Soc.* **445** (2014) 778 [`1408.6953`].

[114] R. J. Cooke, M. Pettini, K. M. Nollett and R. Jorgenson, *The primordial deuterium abundance of the most metal-poor damped Lyα system*, *Astrophys. J.* **830** (2016) 148 [`1607.03900`].

[115] S. A. Balashev, E. O. Zavarygin, A. V. Ivanchik, K. N. Telikova and D. A. Varshalovich, *The primordial deuterium abundance: subDLA system at $z_{\rm abs} = 2.437$ towards the QSO J 1444+2919*, *Mon. Not. Roy. Astron. Soc.* **458** (2016) 2188 [`1511.01797`].

[116] E. O. Zavarygin, J. K. Webb, V. Dumont and S. Riemer-Sørensen, *The primordial deuterium abundance at $z_{abs} = 2.504$ from a high signal-to-noise spectrum of Q1009+2956*, *Mon. Not. Roy. Astron. Soc.* **477** (2018) 5536 [`1706.09512`].

[117] S. Riemer-Srensen, S. Kotu, J. K. Webb, K. Ali, V. Dumont, M. T. Murphy et al., *A precise deuterium abundance: remeasurement of the $z = 3.572$ absorption system towards the quasar PKS1937101*, *Mon. Not. Roy. Astron. Soc.* **468** (2017) 3239 [`1703.06656`].

[118] A. G. Riess, S. Casertano, W. Yuan, L. M. Macri and D. Scolnic, *Large Magellanic Cloud Cepheid Standards Provide a 1% Foundation for the Determination of the Hubble Constant and Stronger Evidence for Physics beyond ΛCDM*, *Astrophys. J.* **876** (2019) 85 [`1903.07603`].

[119] J. L. Bernal, L. Verde and A. G. Riess, *The trouble with H_0*, *JCAP* **1610** (2016) 019 [`1607.05617`].

[120] L. Verde, T. Treu and A. G. Riess, *Tensions between the Early and the Late Universe*, 2019, `1907.10625`.

[121] F. Beutler, C. Blake, M. Colless, D. H. Jones, L. Staveley-Smith, L. Campbell et al., *The 6dF Galaxy Survey: Baryon Acoustic Oscillations and the Local Hubble Constant*, *Mon. Not. Roy. Astron. Soc.* **416** (2011) 3017 [`1106.3366`].

[122] A. J. Ross, L. Samushia, C. Howlett, W. J. Percival, A. Burden and M. Manera, *The clustering of the SDSS DR7 main Galaxy sample ? I. A 4 per cent distance measure at $z = 0.15$*, *Mon. Not. Roy. Astron. Soc.* **449** (2015) 835 [`1409.3242`].

[123] BOSS collaboration, S. Alam et al., *The clustering of galaxies in the completed SDSS-III Baryon Oscillation Spectroscopic Survey: cosmological analysis of the DR12 galaxy sample*, *Mon. Not. Roy. Astron. Soc.* **470** (2017) 2617 [`1607.03155`].

[124] PLANCK collaboration, N. Aghanim et al., *Planck 2018 results. V. CMB power spectra and likelihoods*, `1907.12875`.

[125] D. Blas, J. Lesgourgues and T. Tram, *The Cosmic Linear Anisotropy Solving System (CLASS) II: Approximation schemes*, *JCAP* **1107** (2011) 034 [`1104.2933`].

[126] J. Lesgourgues, *The Cosmic Linear Anisotropy Solving System (CLASS) I: Overview*, `1104.2932`.

[127] T. Brinckmann and J. Lesgourgues, *MontePython 3: boosted MCMC sampler and other features*, `1804.07261`.

[128] B. Audren, J. Lesgourgues, K. Benabed and S. Prunet, *Conservative Constraints on Early Cosmology: an illustration of the Monte Python cosmological parameter inference code*, *JCAP* **1302** (2013) 001 [`1210.7183`].

[129] E. Di Valentino, A. Melchiorri and J. Silk, *Reconciling Planck with the local value of H_0 in extended parameter space*, *Phys. Lett.* **B761** (2016) 242 [`1606.00634`].

[130] E. Di Valentino, A. Melchiorri, E. V. Linder and J. Silk, *Constraining Dark Energy Dynamics in Extended Parameter Space*, *Phys. Rev.* **D96** (2017) 023523 [`1704.00762`].

[131] NASA PICO collaboration, S. Hanany et al., *PICO: Probe of Inflation and Cosmic Origins*, `1902.10541`.

[132] CORE collaboration, E. Di Valentino et al., *Exploring cosmic origins with CORE: Cosmological parameters*, *JCAP* **1804** (2018) 017 [`1612.00021`].

[133] SIMONS OBSERVATORY collaboration, J. Aguirre et al., *The Simons Observatory: Science goals and forecasts*, *JCAP* **1902** (2019) 056 [`1808.07445`].

[134] CMB-S4 collaboration, K. N. Abazajian et al., *CMB-S4 Science Book, First Edition*, `1610.02743`.

[135] K. Abazajian et al., *CMB-S4 Science Case, Reference Design, and Project Plan*, `1907.04473`.

[136] N. Sehgal et al., *CMB-HD: An Ultra-Deep, High-Resolution Millimeter-Wave Survey Over Half the Sky*, `1906.10134`.

[137] E. B. Grohs, J. R. Bond, R. J. Cooke, G. M. Fuller, J. Meyers and M. W. Paris, *Big Bang Nucleosynthesis and Neutrino Cosmology*, `1903.09187`.

[138] LUNA collaboration, D. Trezzi and Trezzi, *Study of the 2H(p,)3He reaction in the BBN energy range at LUNA*, *J. Phys. Conf. Ser.* **940** (2018) 012059.

[139] A. Lagu and J. Meyers, *Prospects and Limitations for Constraining Light Relics with Primordial Abundance Measurements*, 1908.05291.

[140] G. Krnjaic and S. D. McDermott, *Implications of BBN Bounds for Cosmic Ray Upscattered Dark Matter*, 1908.00007.

[141] G. Arcadi, T. Hugle and F. S. Queiroz, *The Dark $L_\mu - L_\tau$ Rises via Kinetic Mixing*, *Phys. Lett.* **B784** (2018) 151 [1803.05723].

[142] P. Foldenauer, *Light dark matter in a gauged $U(1)_{L_\mu - L_\tau}$ model*, *Phys. Rev.* **D99** (2019) 035007 [1808.03647].

[143] N. Okada and O. Seto, *Higgs portal dark matter in the minimal gauged $U(1)_{B-L}$ model*, *Phys. Rev.* **D82** (2010) 023507 [1002.2525].

[144] M. Escudero, S. J. Witte and N. Rius, *The dispirited case of gauged $U(1)_{B-L}$ dark matter*, *JHEP* **08** (2018) 190 [1806.02823].

[145] K. M. Zurek, *Asymmetric Dark Matter: Theories, Signatures, and Constraints*, *Phys. Rept.* **537** (2014) 91 [1308.0338].

[146] K. Petraki and R. R. Volkas, *Review of asymmetric dark matter*, *Int. J. Mod. Phys.* **A28** (2013) 1330028 [1305.4939].

[147] A. Berlin and N. Blinov, *Thermal Dark Matter Below an MeV*, *Phys. Rev. Lett.* **120** (2018) 021801 [1706.07046].

[148] A. Berlin, N. Blinov and S. W. Li, *Dark Sector Equilibration During Nucleosynthesis*, *Phys. Rev.* **D100** (2019) 015038 [1904.04256].

[149] N. Blinov, K. J. Kelly, G. Z. Krnjaic and S. D. McDermott, *Constraining the Self-Interacting Neutrino Interpretation of the Hubble Tension*, 1905.02727.

[150] P. Ilten, Y. Soreq, M. Williams and W. Xue, *Serendipity in dark photon searches*, *JHEP* **06** (2018) 004 [1801.04847].

[151] M. Bauer, P. Foldenauer and J. Jaeckel, *Hunting All the Hidden Photons*, *JHEP* **07** (2018) 094 [1803.05466].

[152] G. Steigman, *Equivalent Neutrinos, Light WIMPs, and the Chimera of Dark Radiation*, *Phys. Rev.* **D87** (2013) 103517 [1303.0049].

[153] Z. Berezhiani, A. Dolgov and I. Tkachev, *BBN with light dark matter*, *JCAP* **1302** (2013) 010 [1211.4937].

[154] P. F. de Salas, M. Lattanzi, G. Mangano, G. Miele, S. Pastor and O. Pisanti, *Bounds on very low reheating scenarios after Planck*, *Phys. Rev.* **D92** (2015) 123534 [1511.00672].

[155] T. Hasegawa, N. Hiroshima, K. Kohri, R. S. L. Hansen, T. Tram and S. Hannestad, *MeV-scale reheating temperature and thermalization of oscillating neutrinos by radiative and hadronic decays of massive particles*, 1908.10189.

[156] M. Kawasaki, K. Kohri, T. Moroi and Y. Takaesu, *Revisiting Big-Bang Nucleosynthesis Constraints on Long-Lived Decaying Particles*, *Phys. Rev.* **D97** (2018) 023502 [1709.01211].

[157] M. Hufnagel, K. Schmidt-Hoberg and S. Wild, *BBN constraints on MeV-scale dark sectors. Part II. Electromagnetic decays*, *JCAP* **1811** (2018) 032 [1808.09324].

[158] L. Forestell, D. E. Morrissey and G. White, *Limits from BBN on Light Electromagnetic Decays*, *JHEP* **01** (2019) 074 [1809.01179].

[159] W. Hu and J. Silk, *Thermalization and spectral distortions of the cosmic background radiation*, *Phys. Rev.* **D48** (1993) 485.

[160] W. Hu and J. Silk, *Thermalization constraints and spectral distortions for massive unstable relic particles*, *Phys. Rev. Lett.* **70** (1993) 2661.

[161] L. Kawano, *Let's Go: Early Universe. Guide to Primordial Nucleosynthesis Programming*, .

[162] L. Kawano, *Let's go: Early universe. 2. Primordial nucleosynthesis: The Computer way*, .

[163] O. Pisanti, A. Cirillo, S. Esposito, F. Iocco, G. Mangano, G. Miele et al., *PArthENoPE: Public Algorithm Evaluating the Nucleosynthesis of Primordial Elements*, *Comput. Phys. Commun.* **178** (2008) 956 [0705.0290].

[164] R. Consiglio, P. F. de Salas, G. Mangano, G. Miele, S. Pastor and O. Pisanti, *PArthENoPE reloaded*, *Comput. Phys. Commun.* **233** (2018) 237 [1712.04378].

[165] T. M. Bania, R. T. Rood and D. S. Balser, *The cosmological density of baryons from observations of 3He+ in the Milky Way*, *Nature* **415** (2002) 54.

[166] E. Vangioni-Flam, K. A. Olive, B. D. Fields and M. Casse, *On the baryometric status of He-3*, *Astrophys. J.* **585** (2003) 611 [astro-ph/0207583].

[167] L. Perotto, J. Lesgourgues, S. Hannestad, H. Tu and Y. Y. Y. Wong, *Probing cosmological parameters with the CMB: Forecasts from full Monte Carlo simulations*, *JCAP* **0610** (2006) 013 [astro-ph/0606227].
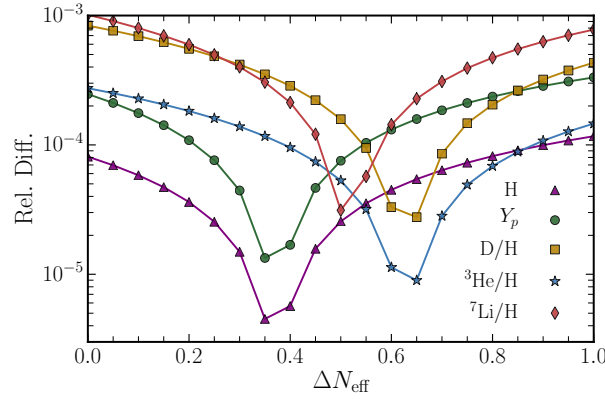
FIG. 6. Relative difference in the primordial abundances between the default version of `PRIMAT` and our modified version of it as a function of ΔN_{eff}. Predictions are done using $\Omega_b h^2 = 0.02225$ and $\tau_n = 879.5$ s.

IX   Appendices

A   Consistency Checks of Modified BBN Code

We checked whether our modifications do not significantly change the values of the primordial helium and deuterium abundances in Standard Model BBN compared to the base version of `PRIMAT`. Table V shows the relative difference in the output of the two codes and it is clear that the accuracy is better than 0.1%.

Abundances	PRIMAT	Modified PRIMAT	Relative Difference (%)
Y_{P}	0.24709	0.24717	0.03
$10^5 \times \text{D/H}|_{\text{P}}$	2.4592	2.4613	0.08

TABLE V. Primordial abundances as computed using `PRIMAT` and our modified version with $\Omega_b h^2 = 0.02225$ and $\tau_n = 879.5$ s.

We also compared our modifications to `PRIMAT` when massless dark radiation is present, which we parametrize in terms of ΔN_{eff}. In `PRIMAT` this is done by increasing N_{eff} directly in the Friedmann equations while in our modified version of the code it is done by including the evolution of a non-interacting, relativistic component. The result is shown in Figure 6. The test shows an accuracy better than 0.1% for all relevant nuclides in the range $0 \leq \Delta N_{\text{eff}} \leq 1$.

B   Comparison with Previous Literature

In this appendix we make a direct comparison between our results and those reported in [97] and [98]. Refs [97] and [98] used a modified version of the Kawano code [161, 162]. In Figure 7, we consider two cases: a Majorana fermion that is purely neutrinophilic or electrophilic. We compute the predictions for helium and deuterium using $\tau_n = 880.1$ s and $\Omega_b h^2 = 0.022$ as in [97] and [98]. We observe a few small differences:

1. Our predicted values of $\text{D/H}|_{\text{P}}$ are smaller than those reported in [97, 98]. Since the difference is WIMP mass independent, we attribute it to updated nuclear reaction rates in `PRIMAT`.

2. The predicted values of Y_{P} are slightly different for $1\,\text{MeV} \lesssim m_\chi \lesssim 15\,\text{MeV}$. The reason is twofold:

   (a) [97, 98] considered that neutrinos decoupled instantaneously and tracked the temperature evolution by using entropy conservation, while we solve for the time evolution of neutrino decoupling. Imposing entropy conservation leads to a feature in the neutrino temperature evolution that affects both the Universe's expansion and the proton-to-neutron conversion rates, see Figure 2 of [103].

   (b) [97, 98] considered instantaneous neutrino decoupling at $T_\nu^{\text{dec}} = 2.0\,\text{MeV}$, while an estimate based on the actual neutrino temperature time evolution yields $T_\nu^{\text{dec}} = 1.91\,\text{MeV}$ [103]. Considering a smaller neutrino decoupling temperature leads to an impact on the proton-to-neutron rates and also reduces the impact of heavier BSM species in neutrino decoupling.

We have also compared our predictions of Y_{P} and $\text{D/H}|_{\text{P}}$ with those reported in [96] (which used `PArthENoPEv1` [163], see [164] for an updated version of the code). We find good overall agreement with [96] and small differences similar to those we find when comparing to [97, 98]. Note that [101] provided updated bounds to those presented in [96] although the predictions for Y_{P} and $\text{D/H}|_{\text{P}}$ are not displayed in that reference.
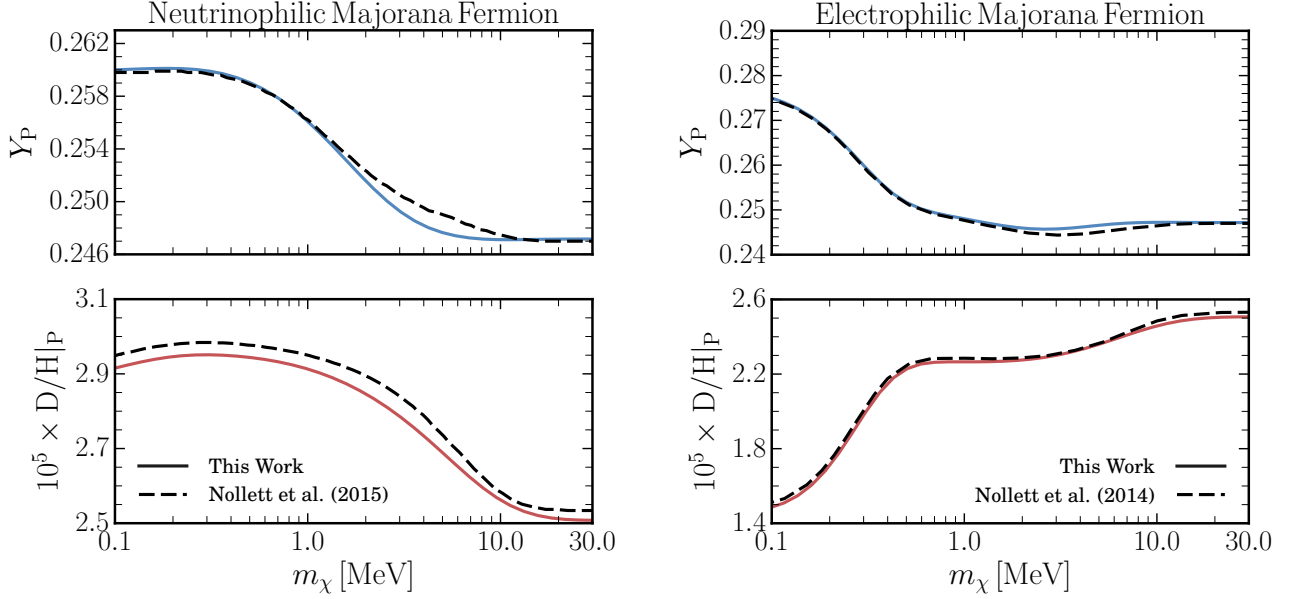
FIG. 7. Comparison with previous literature for the primordial abundances Y_P and $D/H|_P$ as a function of the mass of a Majorana BSM particle that couples exclusively to neutrinos (left panels) or electrons (right panels). The solid lines are from this work and the dashed lines from [97] and [98].

C Conservative Range for the Baryon Density from CMB observations

In the BBN+$\Omega_b h^2$ analysis we consider $\Omega_b h^2 = 0.02225 \pm 0.00066$ to be a conservative and cosmological model independent determination of the baryon energy density by current CMB observations. $\Omega_b h^2 = 0.02225 \pm 0.00066$ has a 4.4 times larger error bar than the one associated with ΛCDM using Planck 2018 observations [7], and furthermore, it covers well the inferred value of $\Omega_b h^2$ in a well-motivated 12-parameter extensions of ΛCDM using different data sets [129, 130]. In Figure 8, one can appreciate that indeed the range with a central value of $\Omega_b h^2 = 0.02225 \pm 0.00066$ covers very well the posterior distributions of $\Omega_b h^2$ of such a 12-parameter extension of ΛCDM including various data sets in conjuntion to Planck CMB observations.
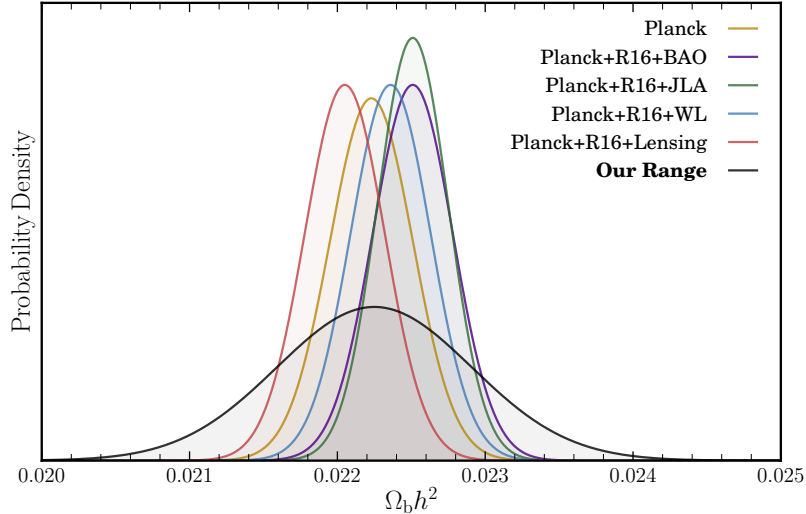
FIG. 8. Illustration of the parameter range for the baryon density we consider in the BBN+$\Omega_b h^2$ analysis as compared to the best-fit values and errors given in Table II of [130]. The authors of [130] infer $\Omega_b h^2$ in a well-motivated 12-parameter extension to ΛCDM using the different data sets shown in the legend. Note in particular that our conservative range for the baryon density encompasses all derived central values and errors.

D Constraints for all Scenarios

In this appendix we display the marginalized $\chi^2(m_\chi)$ for neutrinophilic and electriphilic neutral scalars, complex scalars, Dirac fermions and vector bosons. They can be seen in Figure 9.

We also outline the bounds at 95.4% CL for thermal WIMPs with different annihilation final states to electrons/photons and neutrinos. They are shown in Table VI.

Probe	BSM Particle	$e:\nu$ Annihilation Ratio												
		$1{:}10^6$	$1{:}10^5$	$1{:}10^4$	$1{:}10^3$	$1{:}10^2$	$1{:}10^1$	$1{:}1$	$10^1{:}1$	$10^2{:}1$	$10^3{:}1$	$10^4{:}1$	$10^5{:}1$	$10^6{:}1$
BBN	Majorana	2.2	2.0	1.8	1.8	2.0	2.3	2.4	2.2	1.9	1.6	1.1	0.7	0.5
	Dirac	3.3	2.6	2.2	2.2	2.3	2.4	2.6	2.4	2.1	1.9	1.6	1.1	0.8
	Scalar	1.2	1.2	1.3	1.5	1.7	2.0	2.2	2.0	1.6	1.2	0.8	0.4	0.4
	Complex Scalar	2.2	2.0	1.8	1.8	2.0	2.2	2.4	2.2	1.9	1.6	1.1	0.7	0.5
	Vector	2.9	2.3	2.0	2.0	2.2	2.4	2.5	2.3	2.1	1.8	1.4	0.9	0.7
BBN+$\Omega_b h^2$	Majorana	2.6	2.2	1.8	1.9	2.1	2.4	2.6	2.3	1.9	1.5	1.1	0.9	3.3
	Dirac	4.8	3.0	2.3	2.2	2.4	2.6	2.8	2.5	2.2	1.9	1.5	1.7	6.2
	Scalar	1.3	1.3	1.3	1.5	1.8	2.1	2.3	2.1	1.7	1.2	0.7	0.5	0.6
	Complex Scalar	2.8	2.2	1.8	1.9	2.1	2.4	2.6	2.3	1.9	1.6	1.1	1.0	3.5
	Vector	4.0	2.7	2.1	2.1	2.3	2.5	2.7	2.4	2.1	1.7	1.3	1.5	5.2
Planck	Majorana	8.2	7.6	4.6	3.4	3.6	4.1	4.5	3.8	3.0	2.1	1.1	0.3	4.1
	Dirac	11.0	10.1	6.1	4.0	4.0	4.4	4.8	4.2	3.4	2.4	1.3	0.4; 1.2 - 4.1	7.0
	Scalar	5.4	5.1	3.3	2.8	3.1	3.7	4.1	3.5	2.7	1.8	0.8	-	-
	Complex Scalar	8.3	7.6	4.6	3.4	3.6	4.1	4.5	3.8	3.0	2.1	1.1	0.2	4.3
	Vector	9.8	8.9	5.3	3.7	3.8	4.3	4.7	4.1	3.2	2.3	1.2	0.3; 1.2 - 3.4	6.0
Planck+H_0	Majorana	4.7	3.3	2.0	2.0	2.3	2.7	3.0	3.2	2.5	1.8	0.9	0.2; 0.4 - 8.4	8.9
	Dirac	7.6	5.4	2.6	2.4	2.6	3.0	3.2	3.5	2.8	2.1	1.1; 3.5 - 5.9	0.4; 0.6 - 10.5	11.4
	Scalar	1.6	1.4	1.4	1.6	2.0	2.4	2.7	2.9	2.2	1.5	0.7	0.3 - 5.8	6.2
	Complex Scalar	4.9	3.5	2.0	2.0	2.3	2.7	3.0	3.2	2.5	1.8	0.9	0.2; 0.4 - 8.3	8.9
	Vector	6.6	4.6	2.4	2.2	2.5	2.8	3.1	3.4	2.7	1.9	1.1; 3.4 - 5.4	0.3; 0.5 - 9.7	10.3
BBN+Planck	Majorana	6.4	5.4	3.1	2.7	2.9	3.4	3.7	3.2	2.6	1.9	1.1	7.0	7.8
	Dirac	9.2	7.7	3.9	3.1	3.3	3.6	3.9	3.5	2.9	2.2	1.4	9.3	10.4
	Scalar	3.6	3.2	2.2	2.2	2.6	3.0	3.4	2.9	2.3	1.6	0.8	4.5	5.0
	Complex Scalar	6.5	5.5	3.1	2.7	2.9	3.3	3.7	3.2	2.6	1.8	1.1	7.1	7.8
	Vector	8.2	6.9	3.5	2.9	3.1	3.5	3.8	3.4	2.7	2.0	1.3	8.5	9.4
Simons Obs.	Majorana	12.5	12.3	11.0	7.4	6.3	6.7	7.2	5.8	4.4	2.8	1.3; 1.9 - 10.3	11.9	12.2
	Dirac	15.2	15.0	13.3	8.8	7.0	7.2	7.7	6.4	4.8	3.1	1.6; 2.2 - 12.4	14.6	14.9
	Scalar	9.7	9.6	8.7	6.1	5.5	6.0	6.6	5.4	4.0	2.4	1.0; 1.6 - 8.0	9.3	9.4
	Complex Scalar	12.5	12.3	11.1	7.5	6.3	6.7	7.2	5.9	4.4	2.8	1.3; 1.9 - 10.4	12.0	12.2
	Vector	14.1	13.9	12.4	8.3	6.7	7.0	7.5	6.2	4.7	3.0	1.4; 2.1 - 11.6	13.5	13.8
CMB-S4	Majorana	13.5	13.4	12.4	9.0	7.1	7.4	8.0	6.6	4.8	3.0	1.3; 1.8 - 11.8	13.0	13.2
	Dirac	16.2	16.0	14.7	10.6	8.0	8.1	8.6	7.1	5.3	3.3	1.6; 2.1 - 14.0	15.6	15.9
	Scalar	10.7	10.7	10.0	7.4	6.3	6.7	7.3	5.9	4.3	2.5	1.0; 1.5 - 9.5	10.3	10.5
	Complex Scalar	13.5	13.3	12.4	9.0	7.1	7.4	8.0	6.5	4.8	3.0	1.3; 1.8 - 11.8	13.0	13.2
	Vector	15.1	14.9	13.8	10.0	7.7	7.9	8.4	6.8	5.1	3.2	1.5; 2.0 - 13.2	14.6	14.8

TABLE VI. Lower bounds at 95.4% CL on the masses of various thermal BSM particles in MeV. The bounds are given for a Majorana fermion, Dirac fermion, neutral scalar boson, complex scalar boson and vector boson. The rows correspond to constraints using data from various sources as detailed in Section III. The columns correspond to the ratio of electrophilic to neutrinophilic particles. A '-' means that no bound is obtained at this confidence level and a '# - #' means that masses in this range are excluded.
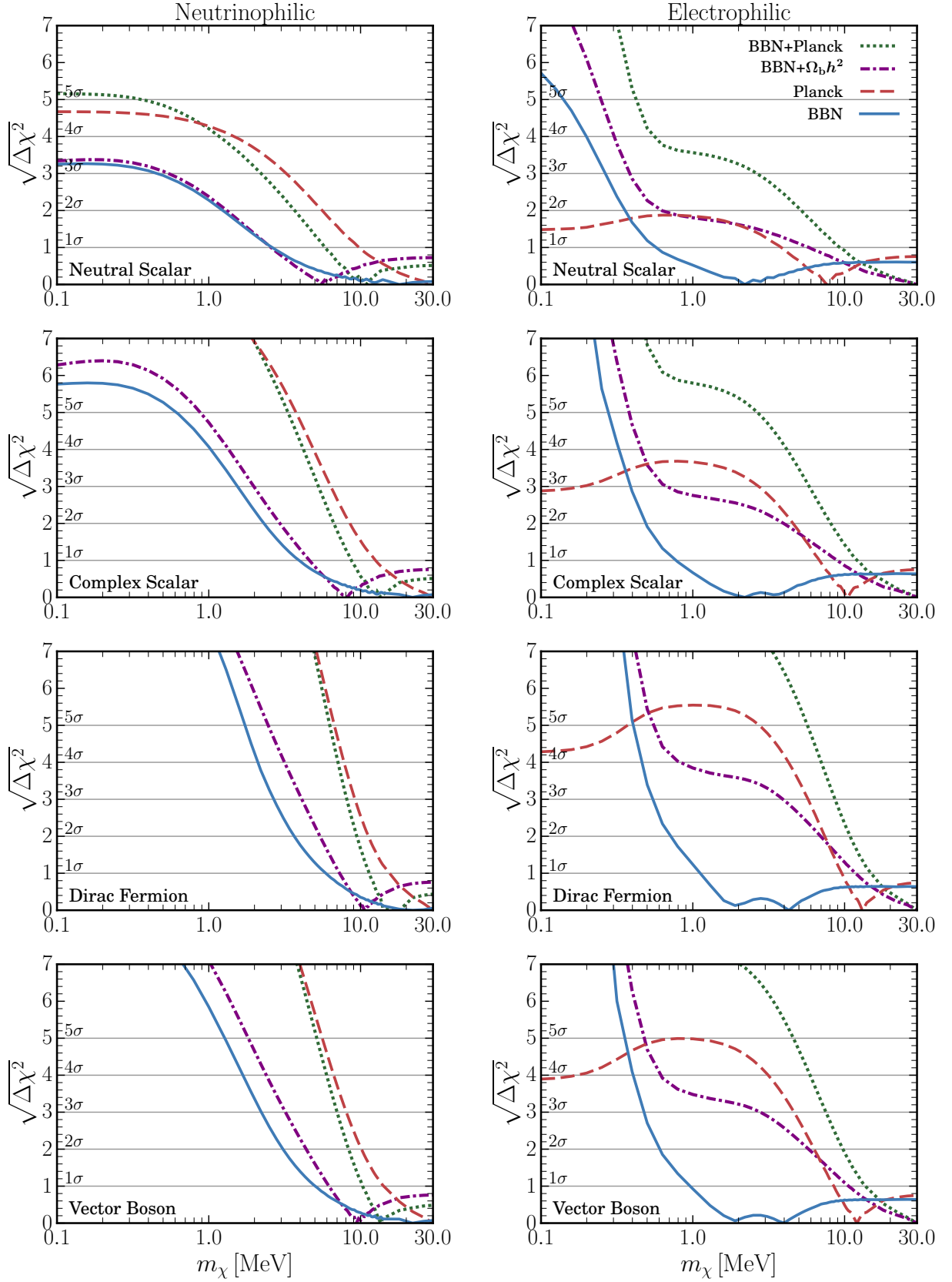
FIG. 9. Additional set of marginalized $\Delta\chi^2$ as a function of the BSM particle mass m_χ. Solid lines correspond to the BBN constraints, the dashed to CMB observations, the dash-dotted to the combination BBN+$\Omega_b h^2$ and the dotted to BBN+CMB. The *left/right panels* correspond to purely neutrinophilic/electrophilic particles.

E Implications for Lithium-7 and Helium-3

We show the evolution of the primordial $^7\text{Li/H}|_\text{P}$ and $^3\text{He/H}|_\text{P}$ abundances in Figure 10 as a function of the mass of a thermal BSM particle. We note that the upper panels do not include any confidence intervals, since it is well known that current measurements of the primordial lithium-7 are in disagreement with SM predictions using the baryon-to-photon ratio inferred from CMB observations [93]. The excluded regions in the lower panels are based on observations of helium-3 in our galaxy [165]. Helium-3 can be both produced and destroyed in stars, which makes it difficult to precisely determine the time evolution of its primordial abundance [166]. Therefore, we have not included measurements of either lithium-7 or helium-3 in our analysis. Nevertheless, if the situation changes in the future, it will be straightforward to obtain bounds from Figure 10 and see how it improves the current BBN constraints.
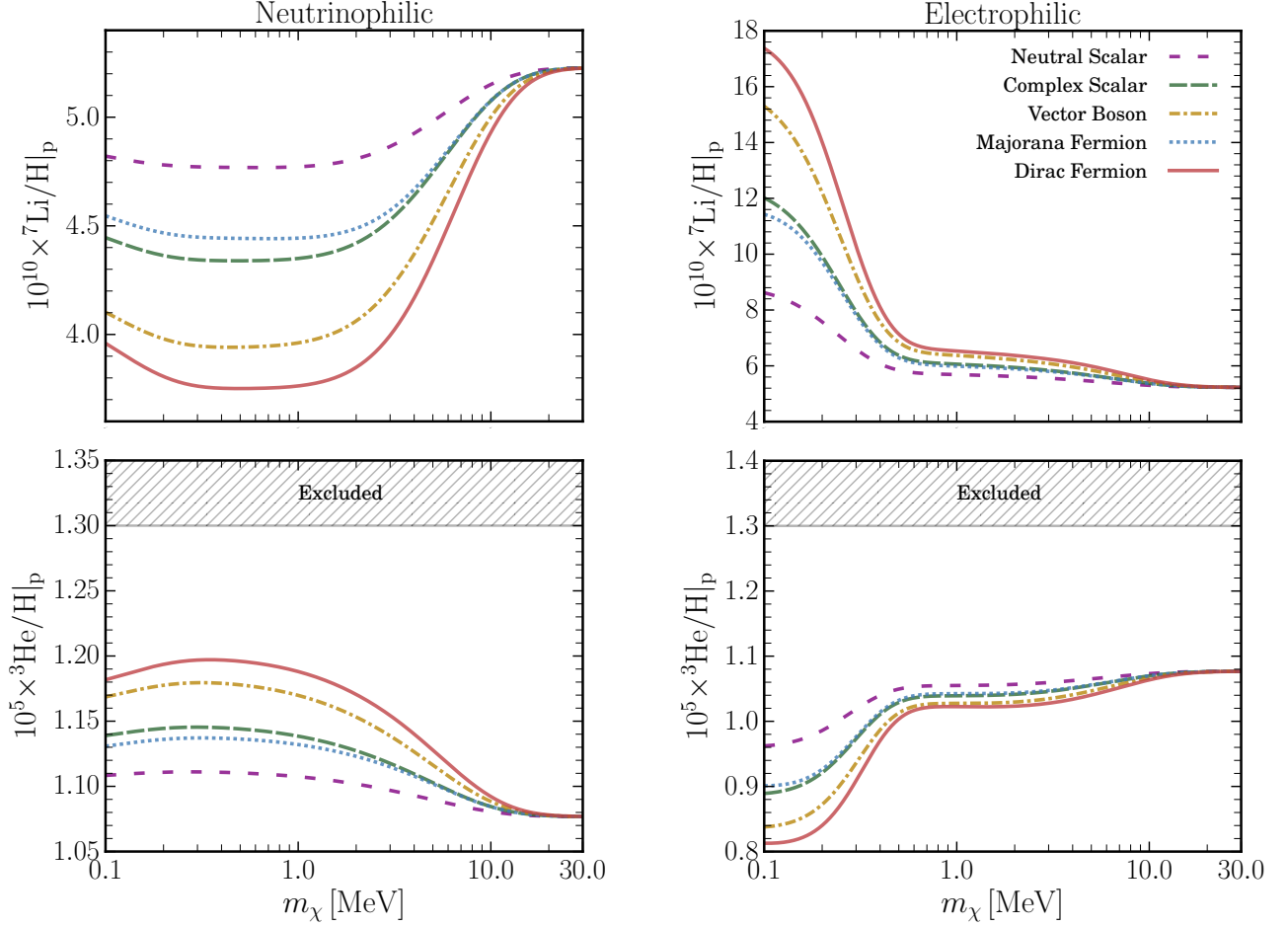

FIG. 10. Cosmological impact of light BSM particles in thermal equilibrium with the SM plasma as a function of their mass m_χ. The *left/right panels* correspond to neutrinophilic/electrophilic particles. *Upper panels:* The lithium-7 primordial abundance $^7\text{Li/H}|_\text{P}$. Measurements of $^7\text{Li/H}|_\text{P}$ are not shown for clarity, see e.g. [93] for current measurements. *Lower panels:* The helium-3 primordial abundance $^3\text{He/H}|_\text{P}$. The grey contours correspond to an upper limit as reported by [165]. The predictions are made with $\Omega_\text{b}h^2 = 0.021875$ and $\tau_n = 879.5\,\text{s}$.

F CMB-S4 Forecast

In order to forecast the reach of CMB-S4 constraints, we first choose a fiducial cosmology with cosmological parameters equal to the Planck 2018 TTTEEE+lowE mean values as in Table 2 of [7], which are reproduced below in Table VII. The fiducial helium abundance is obtained by running `PRIMAT` within the Standard Model and fiducial cosmology.

To forecast the sensitivity of future CMB experiments, we employ the same procedure as used in the CMB-S4 Science Book [134]. Assuming Gaussian statistics, the Fisher matrix for CMB experiments is given by

$$F_{ij} = \sum_{X,Y} \sum_{\ell=\ell_{\min}}^{\ell_{\max}} \frac{\partial \mathcal{C}_\ell^X}{\partial \theta_i} \left[\mathbf{C}_\ell^{XY}\right]^{-1} \frac{\partial \mathcal{C}_\ell^Y}{\partial \theta_i} \ , \tag{19}$$

with indices $X = ab$, $Y = cd$ and $a, b, c, d \in \{T, E, B\}$. The covariance matrix $\mathbf{C}_\ell^{XY}$ for each multipole ℓ is defined as

$$\mathbf{C}_\ell^{abcd} = \frac{1}{(2\ell+1)f_{\mathrm{sky}}} \left[\left(\mathcal{C}_\ell^{ac} + N_\ell^{ac}\right)\left(\mathcal{C}_\ell^{bd} + N_\ell^{bd}\right) + \left(\mathcal{C}_\ell^{ad} + N_\ell^{ad}\right)\left(\mathcal{C}_\ell^{bc} + N_\ell^{bc}\right) \right] \ , \tag{20}$$

with f_{sky} the effective fraction of sky covered by the experiment, $\mathcal{C}_\ell^X$ the simulated CMB power spectra and N_ℓ^X (Gaussian) noise power spectra. The noise is approximated as

$$N_\ell^{aa} = (\Delta X)^2 \exp\left(\frac{\ell(\ell+1)\theta_{\mathrm{FWHM}}^2}{8\ln 2}\right) \ , \tag{21}$$

where $\Delta X \in \{\Delta T, \Delta P\}$ and $N_\ell^{TE} = 0$. We adopt a similar configuration as used in the CMB-S4 Science Book: lensed power spectra with $\ell_{\min} = 30$, $\{\ell_{\max}^{TT}, \ell_{\max}^{TE}\} = 3000$, $\{\ell_{\max}^{EE}, \ell_{\max}^{BB}\} = 5000$, $f_{\mathrm{sky}} = 0.4$, $\theta_{\mathrm{FWHM}} = 1'$, $\Delta T = 1\,\mu$K-arcmin and $\Delta P = \sqrt{2}\,\mu$K-arcmin.

The `CLASS` code [125] is used to obtain the power spectra. The numerical derivatives are computed using the symmetric derivative $\mathcal{C}_\ell'(\theta) = \left[\mathcal{C}_\ell(\theta + \Delta\theta) - \mathcal{C}_\ell(\theta - \Delta\theta)\right]/(2\Delta\theta)$, with fiducial parameter θ and stepsize $\Delta\theta$. The stepsizes used are of order $\Delta\theta_i \sim \sigma(\theta_i)$, as to output a more reliable estimate of the confidence level [167]. The CMB-S4 Fisher matrix is then added to the Planck 2018 low-ℓ TTTEEE+lowP+lowE Fisher matrix to obtain the combined constraints. The fiducial parameters and step sizes used in our computations, together with the forecasted sensitivities, are listed in Table VII. We find good overall agreement with the forecasts performed in [134] within ΛCDM.

Parameter	Fiducial Value	$\Delta\theta$	CMB-S4	CMB-S4+Planck
$\Omega_{\mathrm{b}}h^2$	0.02236	3×10^{-5}	4.9×10^{-5}	4.7×10^{-5}
$\Omega_{\mathrm{c}}h^2$	0.1202	6×10^{-4}	1.8×10^{-3}	1.3×10^{-3}
$100\theta_{\mathrm{s}}$	1.04090	2×10^{-4}	2.3×10^{-4}	1.8×10^{-4}
$\ln(10^{10}A_{\mathrm{s}})$	3.045	9.5×10^{-3}	1.2×10^{-2}	8.1×10^{-3}
n_{s}	0.9649	2×10^{-3}	3.7×10^{-3}	2.9×10^{-3}
τ	0.0544	6×10^{-3}	7.2×10^{-3}	4.8×10^{-3}
N_{eff}	3.046	3×10^{-2}	1.1×10^{-1}	8.1×10^{-2}
Y_{P}	0.2472	4×10^{-3}	6.1×10^{-3}	4.3×10^{-3}

TABLE VII. Forecasted sensitivities of CMB-S4 and CMB-S4+Planck 2018 for the parameters of ΛCDM + N_{eff} + Y_{P}. The column $\Delta\theta$ refers to the stepsizes used to compute the numerical derivatives.